A three-dimensional coupled model of the western Black Sea plankton dynamics: Seasonal variability and comparison to SeaWiFS data

K. P. Tsiaras,[1] V. H. Kourafalou,[2] A. Davidov,[3] and J. Staneva[4]

Received 9 October 2006; revised 2 July 2007; accepted 2 January 2008; published 3 July 2008.

[1] The main physical and biological processes that control the seasonal cycle of the plankton dynamics over the Western Black Sea were explored by means of a three-dimensional, 7-compartment, on-line coupled biophysical model that was developed for this study. Adopting high frequency forcing in terms of air-sea interaction and Danube river inputs, we performed a simulation of the coupled model during the 2002–2003 period. A series of 8-day Chl-a SeaWiFS images provided a validation tool that guided us, along with available in situ measurements, to the improvement of model parameterizations and the calibration of the biological parameters. The simulation of the seasonal phytoplankton variability over the entire Western Black Sea, extending from the highly eutrophic river influenced area to the open sea area, was a major challenge that made necessary the representation of both the spatial and time variability of several processes. Despite the model simplicity, the simulated Chl-a patterns presented a good agreement as compared to the SeaWiFS and in situ data. During winter, phytoplankton in coastal areas was shown to be limited by light availability, primarily due to the increased particulate matter concentrations, as a result of resuspension from the sediment and the increased river loads. During summer, the primary production was mostly sustained by riverine nutrients and regeneration processes and thus was strongly linked to the evolution of the Danube plume. The limiting nutrients showed deviations from the observed concentrations, indicating the necessity for a more realistic phytoplankton growth model.

Citation: Tsiaras, K. P., V. H. Kourafalou, A. Davidov, and J. Staneva (2008), A three-dimensional coupled model of the western Black Sea plankton dynamics: Seasonal variability and comparison to SeaWiFS data, *J. Geophys. Res.*, *113*, C07007, doi:10.1029/2006JC003959.

1. Introduction

[2] The Black Sea is a semi-enclosed basin, connected to the Mediterranean through the narrow and shallow strait of Bosporus. Its hydrodynamics and biogeochemical structure are characterized by a strong main pycnocline, imposed by the hydrological balance that is mostly defined by the fresh river water inflow and the restricted water exchange through the Bosporus straits (outflow of low salinity surface water and inflow of more saline Mediterranean water). The strong density stratification inhibits the ventilation of sub-pycnocline waters. As oxygen is consumed by the decomposition of sinking organic matter, the water mass below ~150 m is permanently anoxic and the distributions of essential nutrients across the oxic/anoxic interface are defined by redox processes.

[3] The Northwestern Black Sea is characterized by a broad shelf and is a highly eutrophic area, as it receives substantial river water discharge from the rivers Dniestr, Dniepr, Bug and particularly the Danube (Figure 1), which contributes to about 70% of the Black Sea fresh water input [*Tolmazin*, 1985]. The significant increase of nitrogen and phosphorus loads from the Danube River during the 1970s – 1980s resulted in the intensive eutrophication of the Northwestern Black Sea shelf which was characterized by the reduction of non-gelatinous zooplankton stocks, mass mortality among benthic communities and decrease of biodiversity [*Zaitsev and Alexandrov*, 1997; *Kideys*, 2002]. The strong eutrophication combined with the invasion of the ctenophore *Mnemiopsis Leidyi* and other synergetic factors such as overfishing [*Gucu*, 2002], led to a significant deterioration of the Black Sea ecosystem and particularly that of the Northwestern shelf area. The recent decrease of nutrient river loads since the beginning of 1990s [*Velikova et al.*, 2005; *Cociacu et al.*, 1997], along with the appearance of a predator of *Mnemiopsis*, the ctenophore *Beroe* [*Finenko et al.*, 2003], have contributed to the gradual recovery of the Black Sea ecosystem [*Kideys*, 2002].

[1] Institute of Oceanography, Hellenic Center for Marine Research, Anavyssos, Greece.
[2] Division of Meteorology and Physical Oceanography, Rosenstiel School of Marine and Atmospheric Science, University of Miami, Miami, Florida, USA.
[3] Biological Oceanography/Marine Biogeochemistry, Leibniz-Institute of Marine Sciences – IFM-Geomar, Kiel, Germany.
[4] Institute for Coastal Research, GKSS Research Center, Geesthacht, Germany.

0148-0227/08/2006JC003959

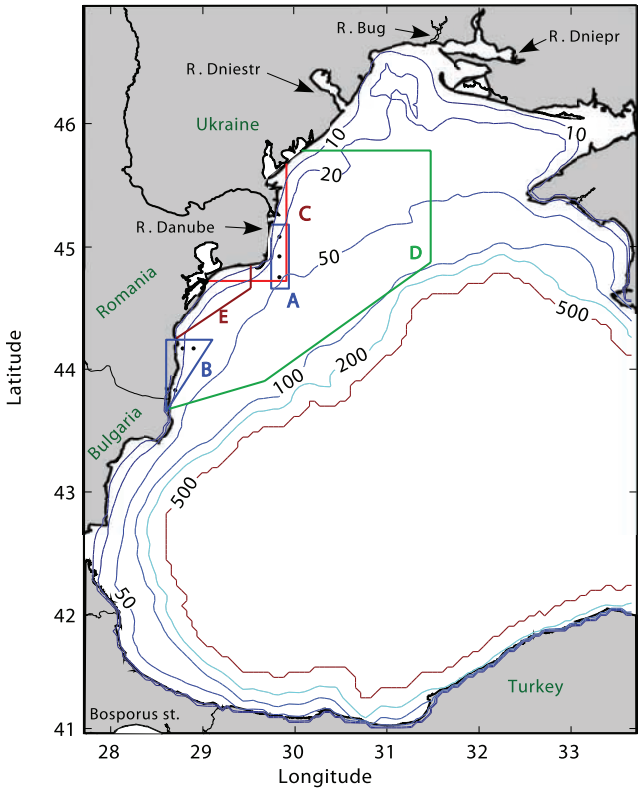

Figure 1. Model domain and bathymetry (isobath depths in m). The Boxes A and B enclose the areas around in situ measurements (indicated as dots) that are compared with area averaged model results (A: Danube prodelta and B: South Romanian Shelf); box C represents the Danube front area (~2400 km^2) where model simulated area averaged sediment fluxes are compared to estimates based on in situ data. The area enclosed by D represents an extended Danube influenced area where average model simulated Chl-a is compared to SeaWiFS; area E represents the North Romanian shelf area that is discussed in the sensitivity studies section (Figure 18).

[4] Over the last decade the Black Sea ecosystem functioning has been explored by several studies, employing models of various complexity levels. A 1-D vertically coupled model of the lower trophic levels was developed by *Oguz et al.* [1996] to study the open Black Sea plankton dynamics and was also used by *Staneva et al.* [1998] to examine the effect of different meteorological conditions. This model was further elaborated by including additional trophic levels [*Oguz et al.*, 1998, 2001a], in order to study food web trophic interactions, resolving redox cycles [*Oguz et al.*, 2001b] and oxygen dynamics [*Oguz et al.*, 2000]. *Oguz and Salihoglou* [2000] expanded the biological model of *Oguz et al.* [1999] to a three-dimensional, three-layer model to assess the impact of the eddy-dominated horizontal circulation on the open Black Sea plankton dynamics. *Eeckhout and Lancelot* [1997] developed a high trophic level resolution 0-D box model to study the functioning of the Northwestern Black Sea shelf ecosystem. The same model was later coupled to a one-dimensional mixed layered model and a three-dimensional hydrodynamic model [*Lancelot et al.*, 2002; *Stanev et al.*, 2002]. *Cokasar and Ozsoy* [1998] investigated the factors that determine the dynamics of different Black Sea regions by implementing variations of the *Fasham et al.* [1990] nitrogen based model. *Lebedeva and Shushkina* [1994] employed a two-layer model to study the effect of *Mnemiopsis* on the Black Sea plankton community. *Gregoire et al.* [1998] developed a three-dimensional coupled biophysical model comprising several size classes of phytoplankton and zooplankton as well as different potentially limiting nutrients (nitrogen, phosphorus, silicate). A somehow simpler nitrogen-based, 6-compartment, three-dimensional coupled model was implemented by *Gregoire et al.* [2004] to study the seasonal variability of plankton and circulation dynamics. The same model was also used to estimate the nitrogen budget of the Northwestern Black Sea shelf [*Gregoire and Friedrich*, 2004]. Even though the few existing three dimensional studies have offered insight on the Black Sea plankton dynamics and certain important coastal processes such as benthic recycling and oxygen dynamics, the current understanding with regard to the processes that control the productivity gradient from the river influenced eutrophic areas to the open sea is still limited.

[5] The primary objective of the present study is to investigate the main physical and biological processes that control the seasonal cycle of the plankton dynamics over the Western Black Sea. The study focus is on the representation of the key processes that determine the productivity gradient from the coastal river influenced areas to the open sea. A three-dimensional, low-trophic level, coupled biophysical model was developed in the framework of the EU DANUBS (DAnube NUtrient management and its impact on the Black Sea, http://danubs/tuwien/ac.at) project. The uncertainties related to the parameterization of several biological processes along with the limitations on temporal and spatial coverage of observations are the main challenges regarding the calibration and validation of a biological model. The satellite-derived chlorophyll-a data by the Sea Wide-Field-of-view Sensor (SeaWiFS) [*McClain et al.*, 2004], which cover the entire area of interest almost continuously, are an extremely valuable tool for this purpose.

[6] Adopting high frequency forcing in terms of air-sea interaction and of the Danube river inputs, we performed a simulation of the coupled model for the period 2002–2003. Following the methodology by A. Davidov (Assessment of algorithms for atmospheric correction and chlorophyll-a retrieval from SeaWiFS satellite data in the western Black Sea area, submitted to *Int. J. Remote Sens.*, 2007) (hereinafter reffered to A. Davidov, submitted, 2007) we analyzed Chl-a SeaWiFS data for the entire year 2003 period and produced a series of images for 8-day averaged patterns. These were employed to improve and assess the model ability to reproduce the observed seasonal primary production variation over the western Black Sea. For model validation, we have also taken into account available in situ measurements (Chl-a, nutrients, inorganic suspended matter, light attenuation) that were obtained during the 2002–2003 period in the Romanian and Bulgarian shelf areas [*Velikova et al.*, 2005; A. Cociasu, unpublished data].

[7] The description of the coupled model and the adopted biological formulations are provided in section 2. In section 3, we present the simulation setup in terms of the

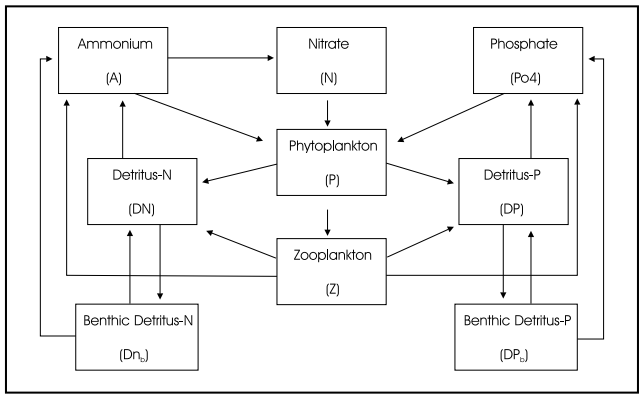

Figure 2. Schematic diagram of the biological model, showing the model state variables and the nitrogen and phosphorus flows among them and across the sediment interface.

employed initial/boundary conditions and forcing. The model results, comparison to data and a series of model sensitivity tests are discussed in section 4.

2. Model Description

2.1. Hydrodynamic Model

[8] The hydrodynamic model is based on the Princeton Ocean Model [*Blumberg and Mellor*, 1983], which is a three-dimensional, sigma-coordinate, primitive equation and free-surface model. A 2.5 turbulence closure submodel [*Mellor and Yamada*, 1982] calculates the vertical eddy viscosity/diffusivity taking into account the wind stirring and the stratification of the water column. The model has been modified to include river plume dynamics, following the approach developed by *Kourafalou et al.* [1996]. This is a key model modification that allows the detailed description of the development and evolution of the Danube River plume. A high-resolution ($\sim$5 km) hydrodynamic model of the Western Black Sea is nested to a lower resolution ($\sim$10 km) basin scale model, which provides the necessary open boundary conditions [*Kourafalou et al.*, 2004]. The model domain is shown in Figure 1. Sixteen sigma levels are resolved in the vertical with logarithmic distribution approaching the surface. In order to increase the vertical resolution in the open Black Sea area, permitting a better simulation of the mixed layer dynamics and the entrainment from the subsurface nutrient pool, we employed a maximum water depth of 500 m. We, therefore, define the ''open sea area'' as the deepest area over the 500 m flat bottom depth. The upper ocean simulated hydrodynamic fields did not show significant differences from those simulated using the hydrodynamic model's initial ''realistic'' bathymetry (with Hmax $\sim$ 2200 m). Therefore since the current study does not concentrate on deep sea circulation details and because vertical processes are particularly important for plankton dynamics in the open sea area, we choose the above approximation for computational efficiency.

2.2. Biological Model

[9] The biological model is a low-trophic level, Fasham type [*Fasham et al.*, 1990], 7-compartment model, which is on-line coupled with the hydrodynamic model of the Western Black Sea. The model compartments consist of: Phytoplankton biomass (P), Zooplankton biomass (Z), Nitrates (N), Ammonium (A), Phosphates ($PO4$), Nitrogen and Phosphorus parts of biogenic Detritus (DN, DP) (Figure 2). The initial model formulation and parameter set was taken by the studies from *Oguz et al.* [1996] and *Staneva et al.* [1998] where a 1-D vertically coupled model was calibrated and tested for the open Black Sea area. Three important modifications were employed to extend the model for application in the river influenced coastal areas.

[10] In the latter studies nitrogen was considered to be the major limiting nutrient. This is a fair approximation for the open Black Sea area where productivity is mostly controlled by the subsurface nutrient pool which is characterized by low N/P ratios due to the removal of nitrogen through the denitrification process that takes place in the suboxic layer [*Murray et al.*, 1989; *Murray et al.*, 2005]. However, the observed N/P ratios [*Cociacu et al.*, 1997; *Ragueneau et al.*, 2002; *Velikova et al.*, 2005] in the Danube influenced waters and river nutrient loads imply a P-limitation and therefore the model was extended to include PO4 and the phosphorus part of detritus as two additional state variables. This was accomplished by adding a phosphorus limitation on the phytoplankton growth function while assuming a fixed N/P stoichiometry for phytoplankton and zooplankton biomass. This may be considered a model simplification at least for phytoplankton, which is known to have more flexible nutrient pools. A Redfield [*Redfield et al.*, 1963] N/P stoichiometry (16:1) was adopted as this is a generally accepted average stoichiometry for marine phytoplankton and zooplankton. However, copepods that often comprise a major portion of zooplankton in the Black Sea are characterized by much higher N/P ratios (20–30) [*Beers*, 1966] while *Hasset et al.* [1997] have shown that both phytoplankton and zooplankton in estuarine regions have a similar N/P ratio of $\sim$20:1. Therefore we have also examined the impact of assigning a higher N/P ratio of 20:1 for both phytoplankton and zooplankton or only zooplankton biomass. Another model upgrade that was proved necessary was the inclusion of a simple benthic model describing the interaction with the sediment in terms of resuspension and deposition of biogenic detritus, as well as the flux of phosphate and ammonium resulting from benthic decomposition. Furthermore, Inorganic Suspended Matter (ISM) was included as a model prognostic variable, in order to more realistically simulate the light conditions within coastal waters, especially during winter, when increased ISM river load and resuspension from the sediment may significantly decrease light availability.

[11] The biological variables are treated as biophysical tracers, subjected to advection, vertical and horizontal diffusion. Therefore the local change of every variable B can be split into a ''hydrodynamic'' part resolved by the hydrodynamic model and a ''biological'' part resolved by the biological model interactions:

$$dB/dt = (dB/dt)_{hydro} + (dB/dt)_{bio} \quad (1)$$

[12] Additional input parameters that are used by the biological model are the photosynthetically active radiation

(PAR) at the sea surface $I(z = 0)$ (which is derived as half the incoming short wave radiation), the water temperature (T), the bottom stress (BS), the inorganic suspended matter concentration (ISM), the water salinity (S) and the water column depth (H).

[13] The local rates of change of the 7 model compartments as defined by the biological interactions within the water column are as follows:

- Phytoplankton

$$\partial P/\partial t = \Phi(I,N,A,PO4,T,P)\ P - G_P(P,DN,Z,T)Z - M_p(P)P$$
$$\text{rate of P change} = \text{growth} - \text{grazing} - \text{mortality} \quad (2)$$

- Zooplankton

$$\partial Z/\partial t = \gamma\, G(P,DN,Z,T)\ Z - M_z(Z,T)Z - R_z(T)Z$$
$$\text{rate of Z change} = \text{growth} - \text{mortality} - \text{excretion} \quad (3)$$

- Detritus-N

$$\partial DN/\partial t = (1-\gamma)G(P,DN,Z,T)Z - G_d(P,DN,Z,T)Z + M_z(Z,T)Z + M_p(P)P - E_N(P,T)DN \pm w_s(DN)\partial DN/\partial z$$
$$\text{rate of DN change} = \text{sloppy feeding} - \text{grazing} + \text{P, Z mortality} - \text{remineralisation} \pm \text{sinking} \quad (4)$$

- Detritus-P

$$\partial DP/\partial t = [(1-\gamma)G(P,DN,Z,T)Z - G_d(P,DN,Z,T)Z + M_z(Z,T)Z + M_p(P)P]/R_{N/P} - E_P(P,T)DP \pm w_s(DP)\partial DN/\partial z$$
$$\text{rate of DP change} = \text{sloppy feeding} - \text{grazing} + \text{P, Z mortality} - \text{remineralisation} \pm \text{sinking} \quad (5)$$

- Nitrate

$$\partial N/\partial t = -\Phi_N(I,N,A,PO4,T,P)\ P + \Omega A$$
$$\text{rate of N change} = -\text{uptake by P} + \text{oxidation of A} \quad (6)$$

- Ammonium

$$\partial A/\partial t = -\Phi_A(I,N,A,PO4,T,P)P + R_z(T)Z + E_N(P,T)DN - \Omega A$$
$$\text{rate of A change} = -\text{uptake by P} + \text{Z excretion} + \text{remineralisation} - \text{oxidation} \quad (7)$$

- Phosphate

$$\partial PO4/\partial t = [-\Phi(I,N,A,PO4,T,P)P + R_z(T)Z]/R_{N/P} + E_P(P,T)DP$$
$$\text{rate of PO4 change} = -\text{uptake by P} + \text{Z excretion} + \text{remineralisation} \quad (8)$$

One should note that the exchange fluxes between phytoplankton/zooplankton and phosphorus variables DP and PO4 in equations (5) and (8) are similar to the nitrogen based equations except they are divided by the assumed constant biomass stoichiometry ($R_{N/P}$). The following equations represent the benthic model interactions between the last water column layer (indexed as b−1) and the bottom layer (indexed as b):

- Phosphate (benthic model)

$$\partial PO4_{b-1}/\partial t = d_{po4}(T,DP_b)$$
$$\text{rate of } PO4_{b-1} \text{ change} = \text{diffusion from the sediment} \quad (9)$$

- Ammonium (benthic model)

$$\partial A_{b-1}/\partial t = d_A(T,DN_b)$$
$$\text{rate of } A_{b-1} \text{ change} = \text{diffusion from the sediment} \quad (10)$$

- Detritus-N (benthic model)

$$\partial DN_{b-1}/\partial t = \left(w_{res}(BS)DN_b - w_{dep}(BS)DN_{b-1}\right)/dz$$
$$\text{rate of } DN_{b-1} \text{ change} = \text{resuspension} - \text{deposition} \quad (11)$$

$$\partial DN_b/\partial t = \left(-w_{res}(BS)DN_b + w_{dep}(BS)DN_{b-1}\right)/dz_b - d_A(T,DN_b) - b\,DN_b$$
$$\text{rate of DN}_b \text{ change} = -\text{resuspension} + \text{deposition} - \text{diffusion of NH4} - \text{burial} \quad (12)$$

- Detritus-P (benthic model)

$$\partial DP_{b-1}/\partial t = \left(w_{res}(BS)DP_b - w_{dep}(BS)DP_{b-1}\right)/dz$$
$$\text{rate of DP}_{b-1} \text{ change} = \text{resuspension} - \text{deposition} \quad (13)$$

$$\partial DP_b/\partial t = \left(-w_{res}(BS)DP_b + w_{dep}(BS)DP_{b-1}\right)/dz_b - d_{PO4}(T,DP_b) - b\,DP_b$$
$$\text{rate of DP}_{b-1} \text{ change} = -\text{resuspension} + \text{deposition} - \text{diffusion of PO4} - \text{burial} \quad (14)$$

[14] The mathematical expressions for the above used functions are described in Table 1, while the employed parameters and the temperature dependence of different processes are given in Tables 2 and 3, respectively. The adopted functions and the choice of the parameter values are briefly discussed below. It should be noted that, as the phytoplankton variability depends both on grazing pressure and phytoplankton growth limitation functions (each one depending on several different processes) the model parameter set cannot be regarded as unique. Furthermore, given the strong impact of many physical processes such as vertical mixing, advection and bottom stress on the ecosystem functioning and the simulated patterns, the parameter calibration would also depend on the hydrodynamic setup, namely the horizontal and vertical resolution as well as the adopted forcing. The parameter values were chosen so as to achieve the best possible fit to the observed phytoplankton seasonal variability, while keeping parameter values as close as possible to those obtained from the available literature.

2.2.1. Phytoplankton

[15] The function $\Phi(I, N, A, PO4, T, P)$ denotes the phytoplankton growth rate and is parameterized according

Table 1. Biological Processes Formulation

Function	Description	Formula
$\Phi(I, N, A, PO4, T, P)$	phytoplankton growth rate	$\sigma_m L_T(T)\ \min\ [L_L(I), L_{NT}(N, A, P), L_{PO4}(PO4, P)]$
$L_T(T)$	temperature dependence	$Q_{10}^{(T-20)/10}$
$L_I(I)$	light limitation	$\tanh\left[\frac{aI(z,t)}{\sigma_m L_T(T)}\right]$
$I(z, t)$	PAR at depth z	$I(z = 0, t)\ \exp\ [-\int k_{tot}\ (z)dz]$
$k_{tot}(z)$	total attenuation coefficient	$k_w + k_p P + k_d D + k_s ISM$
$L_{NT}(N, A, P)$	nitrogen limitation	$L_N(N, A, P) + L_A(A, P)$
$L_N(N, A, P)$	nitrate nitrogen limitation	$\frac{N}{N+K_N(P)}\ \exp\ (-\Psi A)$
$L_A(A, P)$	ammonium nitrogen limitation	$\frac{A}{A+K_A(P)}$
$\Phi_N(I, N, A, PO4, T, P)$	nitrate uptake rate	$\Phi(I, N, A, PO4, T, P)\frac{L_N(N,A,P)}{L_{NT}(N,A,P)}$
$\Phi_A(I, N, A, PO4, T, P)$	ammonium uptake rate	$\Phi(I, N, A, PO4, T, P)\frac{L_A(A,P)}{L_{NT}(N,A,P)}$
$K_N(P)$	nitrate uptake half-saturation	$a_N + b_N P$
$K_A(P)$	ammonium uptake half-saturation	$0.1\ K_N(P)$
$L_{PO4}(PO4, P)$	phosphorus limitation	$\frac{PO4}{PO4+K_{PO4}(P)}$
$K_{PO4}(P)$	phosphate uptake half-saturation	$K_N(P)/16$
$M_p(P)$	phytoplankton mortality	$m_p \frac{P^2}{P^2+K_{mp}}$
$G(P, DN, Z, T)$	zooplankton grazing rate	$\sigma_g L_T(T)\frac{F(P,DN)-F_{th}}{F(P,DN)-F_{th}+K_Z(Z)},\ F > F_{th}$
$F(P, DN)$	total available food for grazing	$p_p(P, DN)(P - P_{th}(P, DN)) + p_d(P, DN)(DN - DN_{th}((P, DN))$
$p_p(P, DN)$, $p_d(P, DN)$	zooplankton preferences for grazing on phytoplankton and detritus	$\frac{P}{P+DN}$, $1 - p_p(P, DN)$
$G_p(P, DN, Z, T)$	zooplankton grazing rate on phytoplankton	$G(P, DN, Z, T)\frac{p_p(P,DN)\cdot(P-P_{th}(P,DN))}{F}$
$G_d(P, Z, T)$	zooplankton grazing rate on detritus	$G(P, DN, Z, T)\frac{p_d(P,DN)\cdot(DN-DN_{th}(P,DN))}{F}$
$P_{th}(P, DN)$, $DN_{th}(P, DN)$	phytoplankton and detritus grazing thresholds	$F_{th}\ p_p\ (P, DN)$, $F_{th}\ p_d(P, DN)$
$K_Z(Z)$	zooplankton grazing half-saturation	$a_Z + b_Z Z$
$M_z(Z, T)$	zooplankton mortality rate	$m_z L_T(T)\frac{Z^2}{Z^2+K_{mz}}$
$R_z(Z)$	zooplankton excretion rate	$\mu_z L_{Tz}(T)$
$E_N(P, T)$	nitrogen remineralization rate	$\varepsilon_N L_T(T)\ f_R(P)$
$E_P(P, T)$	phosphorus remineralization rate	$\varepsilon_P L_T(T)\ f_R(P)$
$f_R(P)$	remineralization phytopl. dependence	$\frac{(0.5+P)}{(0.5+P)+K_r}$
$w_s(DN)$	Detritus sinking rate	$-w_{s\max}\frac{DN}{DN+K_{sd}}$
$w_{res}(BS)$	resuspension rate	$w_{res\max}\left(1 - \frac{\tau_{res}}{BS}\right),\ BS > \tau_{res}$
$w_{dep}(BS)$	deposition rate	$w_{s\max}\left(1 - \frac{BS}{\tau_{dep}}\right),\ BS < \tau_{dep}$
$d_A(T, DN_b)$	ammonium benthic flux	$d_{A\max}L_T(T)\frac{DN_b(S,H)}{DN_{b\max}}$
$d_{PO4}(T, DP_b)$	phosphate benthic flux	$d_{PO4\max}L_T(T)\frac{DP_b(S,H)}{DP_{b\max}}$
$w_s(ISM)$	ISM settling velocity	$0.15(ISM + 0.2)^2$

Table 2. Biological Model Parameter Values

Parameter	Symbol	Value
Phytoplankton maximum growth rate at 20°C	σ_m	3 (day^{-1})
Photosynthesis efficiency parameter	a	0.02 ($(W/m^2)^{-1}$ day^{-1})
Clear water light attenuation coefficient	k_w	0.04 (m^{-1})
Phytoplankton shelf shading coefficient	k_c	0.03 (m^2/mmol N)
Particulate organic matter attenuation coefficient	k_d	0.01 (m^2/mmol N)
Particulate inorganic matter attenuation coefficient	k_s	0.06 (m^2/gr)
NH_4 inhibition parameter	Ψ	3 $(mmol\ N)^{-1}$
Nitrate uptake half-saturation 1st constant	a_N	0.5 (mmol N/m^3)
Nitrate uptake half-saturation 2nd constant	b_N	0.5
Phytoplankton maximum mortality rate	m_p	0.04 (day^{-1})
Phytoplankton mortality half-saturation constant	K_{mp}	0.1 (mmol N/m^3)^2
Herbivore maximum grazing rate at 20°C	σ_g	0.8 (day^{-1})
Phytoplankton threshold conc. for grazing	F_{th}	0.2 (mmol N/m^3)
Grazing half-saturation 1st constant	a_Z	0.2 (mmol N/m^3)
Grazing half-saturation 2nd constant	b_Z	1.3
Herbivore maximum mortality rate at 20°C	m_z	0.45 (day^{-1})
Herbivore mortality half-saturation constant	K_{mz}	0.08 (mmol N/m^3)^2
Herbivore excretion rate at 20°C	μ_z	0.07 (day^{-1})
Herbivore assimilation efficiency	Γ	0.75
Nitrogen maximum remineralisation rate at 20°C	ε_N	0.2 (day^{-1})
Phosphorus maximum remineralisation rate at 20°C	ε_P	0.3 (day^{-1})
Half-saturation for remineral, phytoplankton dependence	K_r	1.5 (mmol N/m^3)
Oxidation rate	Ω	0.05 (day^{-1}), $\sigma_t > 15.4$
Detrital maximum sinking rate	$w_{s\max}$	4 (m/s)
Half-saturation for detritus sinking	K_{sd}	0.2 (mmol N/m^3)
Detrital maximum resuspension rate	$w_{res\max}$	0.006 (day^{-1})
Critical shear stress for resuspension	τ_{res}	0.01 (Nt/m^2)
Critical shear stress for deposition	τ_{dep}	0.4 (Nt/m^2)
Maximum ammonium benthic flux	$d_{A\max}$	1 (mmol N m^{-2} day^{-1})
Maximum phosphate benthic flux	$d_{PO4\max}$	0.15 (mmol P m^{-2} day^{-1})
Initial benthic pool maximum nitrogen conc.	$DN_{b\max}$	(100 mmol N m^{-2})
Initial benthic pool maximum phosphorus conc.	$DP_{b\max}$	(6.25 mmol P m^{-2})
Sediment burial rate	B	0.007 (day^{-1})
Phytoplankton and zooplankton N/P stoichiometry	$R_{N/P}$	16

to the Liebig's law of the minimum, assuming that either light or nutrient limitation (but not both) controls phytoplankton growth [*Oguz et al.*, 1996]. A temperature dependence is assigned to the maximum growth rate following *Eppley* [1972]. The light limitation $L_I(I)$ is parameterized according to *Jassby and Platt* [1976], assuming that the photosynthesis efficiency parameter a is constant.

[16] Photosynthetically available radiation $I(z)$ is assumed to decrease exponentially with depth. The total attenuation coefficient $k_{tot}(z)$ is split into contributions by clear water (k_w), phytoplankton shelf-shading (k_c), organic (k_d) and inorganic (k_s) particulate matter. In the work of *Oguz et al.* [1996] the values for the attenuation of water $k_w = 0.08$ and phytoplankton $k_c = 0.07$ were chosen in order to fit light attenuation observations in the open sea during spring and summer [*Vidal*, 1995; *Vladimirov et al.*, 1996]. Since inorganic particulate matter is now a model variable, we used lower attenuation values $k_w = 0.04$ and $k_c = 0.03$ according to *Fasham et al.* [1990] and *Lorenzen* [1972]. We chose the values for organic (k_d) and inorganic (k_s) particulate matter $k_d = 0.01$, $k_s = 0.07$, based on a best fit to the observed Chl-a patterns during winter light limited periods, while keeping simulated k_{tot} values in the open sea close to those from *Oguz et al.* [1996] (see also discussion later). In that way we tried to provide a more realistic description of the seasonal variability for light conditions within coastal waters, which are expected to be more turbid during winter, due to the increased resuspension and river load of particulate matter.

[17] The nitrogen limitation function is based on *Wroblewski* [1977] and accounts for the inhibition of nitrate uptake in the presence of ammonium.

[18] A present study innovation is the adoption of a variable half-saturation function (rather than constant) for nutrient uptake, as well as for zooplankton grazing that will be discussed later. The most frequently used formulation, along with internal storage formulations [e.g., *Droop*, 1968], is the one introduced by *Monod* [1942], which has the form:

$$V = V_{\max} * \frac{NUT}{NUT + K} \tag{15}$$

where NUT is the nutrient concentration and K is the half-saturation constant representing the nutrient concentration where the uptake rate V reduces to half its maximum value $V_{\max}$. This formulation was confirmed for monospecific cultures under steady state conditions and is a generally accepted model describing a single-species nutrient uptake mechanism [*Button*, 1978]. The half-saturation constant has been calculated for many different species [e.g., *MacIsaac and Dugdale*, 1969; *Eppley et al.*, 1969] and may vary significantly according to the nutrient environment to which they are adapted. Different ($V_{\max}$, K) values are a way to explain resource competition among species [*Dugdale*, 1967; *Tilman*, 1981]. In oligotrophic environments, for example, a low K value adaptation (usually with the cost of having a lower $V_{\max}$) permits the cell to grow faster under

Table 3. Temperature Dependence (Q_{10}) of Biological Processes

Biological Process	Q_{10} Value
Phytoplankton growth	1.88
Zooplankton growth	1.88
Zooplankton mortality	2.2
Zooplankton excretion	1.88
Remineralization	1.2
Benthic flux of phosphate, ammonium	1.2

lower nutrient concentrations and thus to dominate against other species with higher K values. A natural system that is characterized by significant spatial and/or time variability in terms of nutrient conditions and subsequently of species composition cannot be described by a single K value Monod equation. Deviations from the Monod kinetics have been shown for mixed populations with different K values [*Williams*, 1973; *Tarapchak and Herche*, 1986], especially when the relative species abundances are significantly different [*Tarapchak and Herche*, 1986].

[19] An alternative formulation adopting a variable half-saturation function, rather than constant, was introduced by *Contois* [1959]:

$$V = V_{\max} * \frac{NUT/P}{NUT/P + b} = V_{\max} * \frac{NUT}{NUT + b * P} = V_{\max} * \frac{NUT}{NUT + K(P)} \quad (16)$$

The nutrient uptake rate in this case depends rather on the ratio of available nutrients per unit phytoplankton biomass NUT/P or equivalently, the half-saturation function increases linearly with biomass. The Contois formulation was shown to better describe nutrient uptake in mixed cultures, while its predicted negative dependence of growth rate on biomass concentration was attributed to the accumulation of inhibitory metabolic by-products (review by *Jost* [2000]). In the present study context, the Contois formulation provides a means of adjusting nutrient uptake according to the actual nutrient conditions assuming an adaptation of the dominant species to these conditions. As pointed out by *Morrisson et al.* [1987], this formulation seems to be more suitable than the Monod expression for non-homogenous systems (many species, nutrient gradients etc). In the present study an intermediate function $K(P) = a + b * P$ (which reduces to Monod for $P = 0$) was adopted, that is similar to *Roques et al.* [1982]. Setting a lower limit for the half-saturation function signifies some kind of threshold for nutrient uptake.

[20] The phytoplankton mortality is parameterized using a sigmoid function according to *Ryabchenko et al.* [1997] in order to increase the model stability.

2.2.2. Zooplankton

[21] The equivalent of the Monod formulation was introduced by *Holling* [1959] to describe the variability of zooplankton grazing rate on phytoplankton concentration:

$$G = G_{\max} * \frac{P}{P + K_Z} \quad (17)$$

K_Z is the half-saturation constant where the grazing rate G reduces to half of its maximum value $G_{\max}$. This formulation reflects the saturation of the attack rate as phytoplankton concentration increases, because of the finite number of preys the predator can handle. The above formulation has been criticized because it predicts an increase of only the herbivore biomass (of two trophic levels in our case) in response to an increase of phytoplankton growth rates, while in natural systems abundances of all trophic levels are expected to vary proportionally (review by *Ginzburg and Akcakaya* [1992]). *Arditi and Ginzburg* [1989] and *Arditi and Akcakaya* [1990] proposed that a way to resolve this paradox is to describe the predator attack rate as a function of the prey/predator concentration ratio P/Z (which is equivalent in form to the Contois function for nutrient uptake) as a result of predator mutual interference. This concept of decreasing grazing efficiency in higher predator densities was also earlier introduced by *DeAngelis et al.* [1975]. Using such a "ratio dependent" function prevents the occurrence of limit cycles that are a symptom of using the Holling formulation. During our preliminary simulations, using the Holling formulation resulted in a significant underestimation of phytoplankton concentration and the occurrence of unrealistically large amplitude oscillations that were prevented only after a significant reduction of the maximum grazing rate. *Gregoire et al.* [2004] also mentioned that a 10-fold increase in phytoplankton growth rates was reflected by only a zooplankton stock increase, which also sounds like a symptom of using the Holling formulation. Trying to avoid such an unrealistic variability led us to the adoption of a formulation that is similar to the one proposed by De'Angelis (the equivalent of *Roques et al.* [1982] for nutrient uptake) which is an intermediate model reducing to Holling for low zooplankton values:

$$G = G_{\max} * \frac{P}{P + a_z + b_z * Z} \quad (18)$$

The above function has been generalized in order to include zooplankton grazing on both phytoplankton and detritus. The zooplankton preference functions are assumed to depend on the relative phytoplankton and detritus concentrations following *Fasham et al.* [1990].

[22] *Steele and Henderson* [1992] revealed the importance of the zooplankton mortality (as a closure term of an NPZ model) parameterization on the overall ecosystem dynamics. The zooplankton mortality can be expected to increase with increasing zooplankton density, as a result of a higher predator whose biomass may be assumed to vary proportionally to its prey [*Steele and Henderson*, 1981] or as cannibalism, including predation between different species that comprise the same aggregated zooplankton compartment [*Kohlmeier and Ebenhoh*, 1995]. The "s-shaped" function that we have adopted for the zooplankton mortality rate may be interpreted to represent a satiable higher-predator that reduces its searching efforts for low prey concentrations [*Edwards and Yool*, 2000]. A temperature dependence ($Q_{10} = 2.2$) was also assigned in our formulation permitting the representation of the "higher predator's" seasonal cycle. The choice of zooplankton mortality parameters (m_z, K_{mz}, Q_{10}) was based on the best fit of the phytoplankton seasonal variability as deduced by our model and SeaWiFS observations.

[23] Given the strong control exerted by higher predators on zooplankton communities [e.g., *Oguz et al.*, 2001a; *Lebedeva and Shushkina*, 1994], particularly in the eutrophic Northwestern shelf area, the parameterization of zooplankton mortality plays a significant role in simulating the phytoplankton variability. The adopted parameterization, even though unable to capture the time variability that arises from the trophic interactions and the different physiology (temperature dependence, functional response, repro-

duction patterns) of the different groups that comprise the assumed "higher predator", provides a reasonable first approximation in the context of the present model simplicity and overcomes problems of underestimated phytoplankton biomass in the river influenced eutrophic waters that were encountered by *Gregoire et al.* [2004].

[24] Adopting a variable mortality rate provides a means to prevent the occurrence of unrealistic limit cycles [*Steele and Henderson*, 1992; *Edwards and Yool*, 2000] while keeping the Holling formulation for zooplankton grazing. In fact, the choice of the grazing formulation has no significant impact on phytoplankton biomass in the productive river influenced waters, where the increased zooplankton predation mortality results in a quite low grazing pressure. However, zooplankton mortality is a "top-down" control defined by the biomass of higher predators that may depend on external factors (such as top-predation, temperature, anoxia etc). Adopting the "ratio-dependent" grazing formulation, which introduces a "bottom-up" negative feedback mechanism increased the model stability and robustness even under lower zooplankton mortality rates (see discussion of model results in section 4).

2.2.3. Detritus

[25] Microbial decomposition of particulate and dissolved organic matter (comprising the detritus compartment) is likely to proceed at much higher rates within coastal eutrophic areas. The detritus decomposition rate therefore is assumed to increase with increasing phytoplankton concentration, since the bacteria biomass, which is not explicitly represented, can be expected to follow an algal biomass increase and the subsequent production of Particulate Organic Matter (POM). A similar model formulation was proposed by *Di Toro and Matystik* [1980]; the difference in our model formulation is that we set a lower limit in the remineralisation rate for low phytoplankton concentrations. Significant correlation between decomposition rates and photosynthesis has also been recorded from in situ measurements [e.g., *Harrison*, 1978]. We chose using phytoplankton rather than detritus as the depending variable, because fresh organic matter is expected to decompose at much faster rates. *Garber* [1984] indicates decomposition rates of 0.02–0.2 day^{-1} for the more labile fraction of POM. A maximum rate of 0.2 day^{-1} was assigned for nitrogen (in the open sea the nitrogen remineralization rate reduces to $\sim$0.05 day^{-1} on average as by *Oguz et al.* [1996]) while a higher value of 0.3 day^{-1} was fitted for phosphorus. Higher decomposition rates for Phosphorus have been shown to occur at least during the initial phase of decomposition [*Garber*, 1984; *Grill and Richards*, 1964] and are also suggested by the increase of dissolved and particulate organic matter N/P stoichiometry over depth [*Hopkinson et al.*, 2002; *Knauer et al.*, 1979].

[26] The detritus sinking velocity can be expected to increase at higher concentrations as a result of flocculation. Therefore a hyperbolic function is adopted as by *Oguz et al.* [2001a].

2.2.4. Benthic Model

[27] An initial organic matter benthic pool (DP_{b0} (S, H), DN_{b0} (S, H)) was assumed to vary as a function of the annual mean surface salinity and water column depth (therefore, higher values were assigned in river influenced coastal areas). The deposition and resuspension rates of biogenic detritus from this sediment pool are calculated as functions of the bottom stress, which is provided by the hydrodynamic model [*Guan et al.*, 2001]. The employed function for erosion is based on *Partheniades* [1965] while the deposition formulation is based on *Krone* [1962].

[28] Benthic decomposition is parameterized assuming a temperature dependent diffusional flux of phosphate and ammonium from the sediment pool. The maximum benthic fluxes (0.15 mmol P m^{-2} day^{-1} for phosphate and 1 mmol N m^{-2} day^{-1} for ammonium) were assigned taking into account the *Friedrich et al.* [2002] estimates from in situ measurements within the Danube front area [*Friedrich et al.*, 2002, Figure 8] during summer 1995 and spring 1997 (see also discussion in section 4).

[29] The assigned values for the maximum benthic pool concentrations (100 mmol N/m^{-2}; 6.25 mmol P/m^{-2}) were chosen so as to achieve a reasonable seasonal variability of the benthic pool and the associated benthic fluxes in response to the deposition/resuspension variability. Assigning much higher values would make the benthic pool practically constant, while lower values would result in unrealistic short term variability.

2.2.5. Inorganic Suspended Matter

[30] The ISM is subjected to resuspension and deposition using the same formulation as for biogenic detritus. The assumed initial sediment pool however, is defined assigning a smaller weight on salinity and a larger weight on water column depth. The dependence of the ISM settling velocity on flocculation was parameterized using a function of only ISM concentration of the form $w = a * (ISM)^b$ [*Krone*, 1962; *Dyer*, 1989; *Shi and Zhou*, 2004]. Additional dependencies on shear stress [*Burban et al.*, 1989] and salinity would be probably necessary for a more accurate sediment transport model that is beyond the scope of this study. We should note that given the simplicity of the sediment transport model, some deviations of the light attenuation coefficient (k_s) fitted value would be expected, as this strongly depends on the simulated ISM concentration.

3. Simulation Setup

3.1. Forcing

[31] The air-sea interaction for the 2002–2003 period was based on 6-hourly meteorological forcing with $\sim$10 km horizontal resolution, provided by the operational atmospheric model of the Hellenic Center for Marine Research POSEIDON Project [*Papadopoulos et al.*, 2002] (http://www.poseidon.ncmr.gr/). Such high-frequency and high-resolution atmospheric forcing was particularly valuable for the simulation needs, as it permitted the capture of the high variability in the Danube plume transport pathways. The provided meteorological data included 10 m wind speed, 2 m air temperature, 2 m relative humidity, precipitation, incoming long-wave radiation and incoming short-wave radiation. These data were used by the hydrodynamic model to evaluate the surface heat, water and momentum fluxes using similar bulk formulas (sensible and evaporative heat fluxes after *Rosati and Miyakoda* [1988]; turbulent exchange coefficients after *Kondo* [1975]; wind stress after *Hellermann and Rosenstein* [1983]) to what has been adopted by the POSEIDON operational hydrodynamic

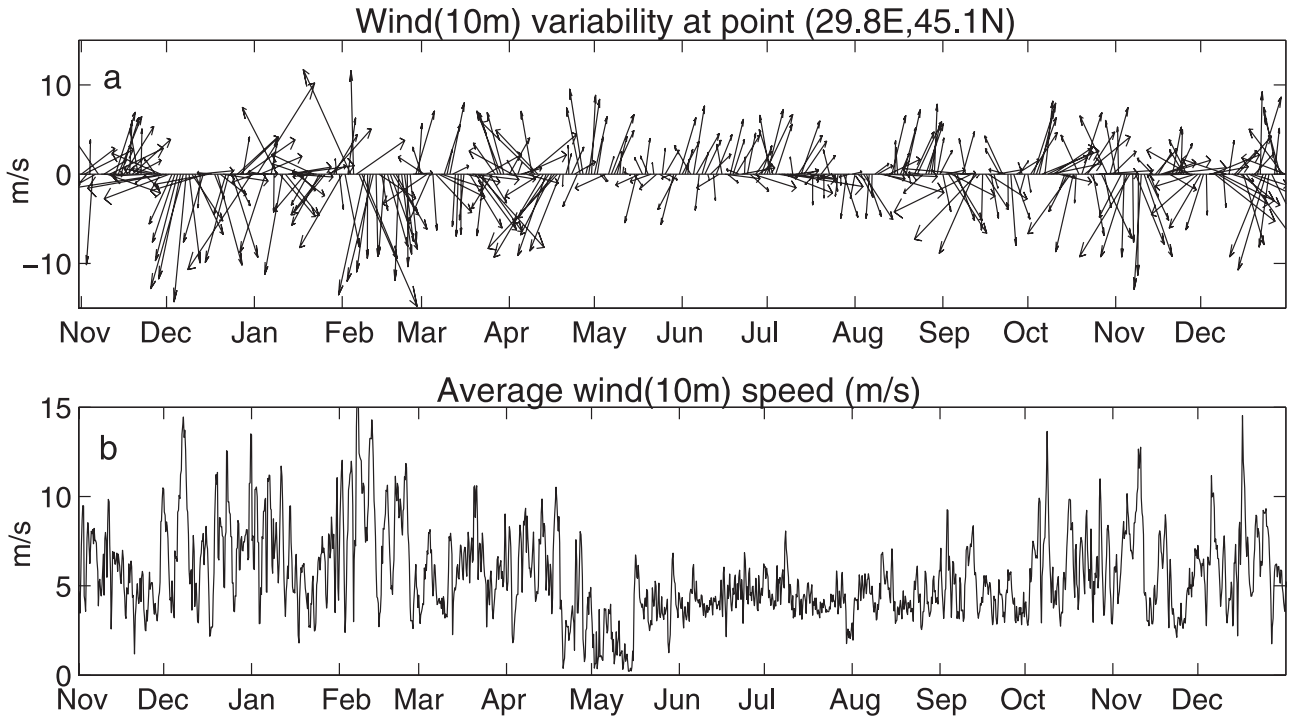

Figure 3. (a) Wind (10 m) variability in the Danube front area (29.8°E, 45.1°N) and (b) wind speed (m/s) variability averaged over the Western Black sea, for the 2002–2003 period (the fields are provided by the POSEIDON operational atmospheric forecast model).

model [*Nittis et al.*, 2006]. The incoming short wave radiation was also used as an input parameter in the biological model. In Figure 3 we can see the wind variability in the Danube front area and the variability of the average wind speed over the Western Black Sea area.

[32] Daily Danube discharge rates and nutrient inputs (Figure 4) were calculated by a model of the Danube Delta [*Constantinescu and Menting*, 2000; *Gils et al.*, 2005] based on estimated nutrient emissions by a model of the Danube catchment area [*Schreiber et al.*, 2005] and measurements. The N/P ratio of the Danube input for 2003 (not shown) has a lower value of 30 during summer 2003 and a maximum above 100 during winter. Therefore, phosphate is expected to be the most limiting nutrient in river-influenced waters. For the other major Western Black Sea rivers (Dniepr, Bug, Dniestr) we employed constant values of discharge rates based on climatology by *Kourafalou and Stanev* [2001]. The dissolved inorganic nitrogen and phosphate concentrations were assigned to 1/10 and 1/5 of the respective Danube concentrations, giving a total load of about 3% for nitrogen and 7% for phosphorus of the Danube inputs, as suggested by *Friedl et al.* [1998].

3.2. Initial and Boundary Conditions

[33] The initial conditions (temperature, salinity and biological variables) for the 2002–2003 simulation were provided by a 1-yearlong climatological type simulation of the coupled model under perpetual year daily mean air-sea fluxes with high frequency anomalies superimposed. For a full description of the hydrodynamic long-term simulation see *Kourafalou et al.* [2004]. The air-sea fluxes as well as the initial density field were provided by a long-term climatological run of a basin scale hydrodynamic model [*Staneva and Stanev*, 1997]. On the other hand, the Danube discharge rates and nutrient inputs were assigned to their 2001–2002 year period values in order to approximate the actual nutrient conditions in the beginning of the 2002–2003 simulation.

[34] For this climatological type simulation the initial conditions of the biological state variables were obtained by simulating the vertical profiles with a 1-D version of the coupled model that was based on *Oguz et al.* [1996] and then adopting a density dependent interpolation on our 3-D coupled model grid. Using density rather than depth for the interpolation into the model grid is aiming at the exclusion of the horizontal variability due to dynamical effects [*Tugrul et al.*,. 1992; *Saydam et al.*, 1993]. In order to provide an initial representation of the eutrophic riverine waters, the nutrients concentrations were further assigned a linear increase with salinity from the open sea to the river end (Nitrates: $N = N_0 + 2.5 * (18 - S)$, Phosphates: $PO4 = PO4_0 + 0.1 * (18 - S)$, $S < 18$). This can be considered their dilution conservative mixing variation [*Humborg*, 1997; *Ragueneau et al.*, 2002]. The rates for the assigned increase with salinity for nitrate and phosphate were chosen so that the river end concentrations would roughly agree to measurements at the Danube outflow area during 2001–2002 (A. Cociasu, personal communication). In proportion, a combined function of salinity and water column depth was used to describe the initial sediment nutrient pool. The initial nitrate and phosphate vertical profiles in the open sea were fitted to the data obtained by the Knorr campaign on April 2003 (www.ocean.washington.edu/cruises/Knorr2003), that revealed a value of $\sim$4 μM for

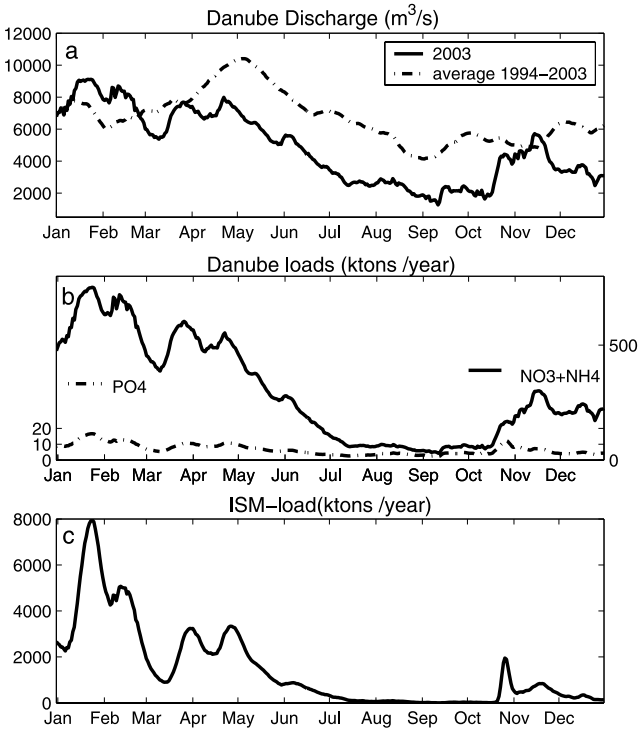

Figure 4. (a) Danube discharge variability over 2003 (solid line). The dash-dot line represents a long term average over the 1994–2003 period (A. Constantinescu, unpublished data), (b) dissolved inorganic nitrogen (solid line) and phosphorus (dash-dot line) Danube loads (ktons/a) variability. Notice that the scaling on *Y* axis is fitted to N/P molar ratios of 16:1 (i.e., the two lines coincide when N/P ratio equals 16:1), (c) Inorganic suspended matter Danube load (ktons/a).

the nitrate subsurface maximum concentration. The subsurface nitrate pool has been shown to exhibit a significant inter-annual variability in response to the variation of primary production and the subsequent fluxes of organic matter in the water column [*Konovalov et al.*, 2005]. Nitrate maximum values of ~6 μM, ~12 μM and ~3 μM have been recorded during 2001, 1991 and 1969 respectively.

[35] Since the model vertical resolution does not permit a proper representation of the subsurface nitrate maximum, a constant value was assigned below this maximum in order to prevent the establishment of artificial horizontal variability. Consequently, the removal of nitrates through denitrification has not been taken into account.

[36] The values of biological variables along the open eastern boundary are relaxed to an area average over the open sea along isopycnal surfaces. In that way we avoided a simulation of the coupled model over the entire Black Sea that would significantly increase the computational time. Instead, a lower resolution (~10 km) basin scale hydrodynamic model simulation provides the necessary input for the hydrodynamic variables open boundary conditions, which are as follows. The integrated (barotropic) velocity is calculated using a *Flather* [1976] type radiation condition. Temperature and salinity are calculated from their upstream values during outflow and prescribed boundary values from the basin scale model during inflow, using an advection equation. Finally, internal (baroclinic) velocities are assigned to the prescribed boundary values from the basin scale model.

4. Discussion of Results

4.1. Seasonal Variability of Hydrodynamic Fields

[37] The circulation on the Northwestern Black Sea shelf is controlled by air-sea and land-sea interaction processes, while topographic controls and offshore flows also play a prominent role. As is known from several previous observational and modeling studies [e.g., *Stanev et al.*, 1997; *Oguz et al.*, 1992, 1995; *Oguz and Malanotte-Rizzoli*, 1996; *Staneva and Stanev*, 1998; *Korotaev et al.*, 2003], the atmospheric fluxes control the basin scale thermohaline circulation and the formation of the Cold Intermediate Layer (CIL), while the wind stress curl is the driving mechanism for the topographically induced Rim Current system and associated eddies along the basin's shelf break. The formation and development of the river plumes on the broad Northwestern shelf impose a major control on the coastal circulation, as demonstrated by *Kourafalou and Stanev* [2001] and *Kourafalou et al.* [2004]; see Figure 1 for river locations.

[38] During the present study 2002–2003 simulation with high frequency forcing, the hydrodynamic fields exhibited the above known circulation characteristics and allowed a close look at the seasonal variability. Examples of near surface salinity and current velocity are given on Figure 4 for weekly averages that match the dates employed by satellite data that will be used for model validation of chlorophyll fields at a later section. The model simulated patterns are greatly influenced by the variability in the realistic wind and buoyancy forcings shown at Figures 3 and 4, respectively. A dominant circulation feature is the Danube River plume, characterized by an anticyclonic bulge near the delta. Secondary plumes associated with the Dniestr, Bug and Dniepr rivers contribute to the low salinity coastal waters on the Northwestern shelf.

[39] During winter (Figure 5a) a well-pronounced Rim Current flows around the basin, close to the shelf break slope. The winds are strong and with a prevailing direction from the north to northeast. Both buoyancy and wind-forcings encourage the formation of a southward coastal current along the western coast. Similar to the discussion of satellite data by *Korotaev et al.* [2003], a strong cyclonic cell of the western gyre is found north of the Rim Current between about 29°E and 30°E, while a well-pronounced anticyclonic Sakarya eddy is found south of the Rim Current at about 31°E, over the area of strong along-shore topographic variation (Figure 1). Following the spring period of maximum river discharge, the late spring (May, Figure 5b) and late summer (June, Figure 5c) salinity distributions have strong river plumes and anticyclonic circulation in the coastal area near the Danube delta. The Rim Current is still evident in May, starting to diminish in June, due to the weakening of the wind field. The onset of seasonal stratification and the shift of the winds to a northeastward direction allow a strong expansion of the near surface, river induced low salinity coastal

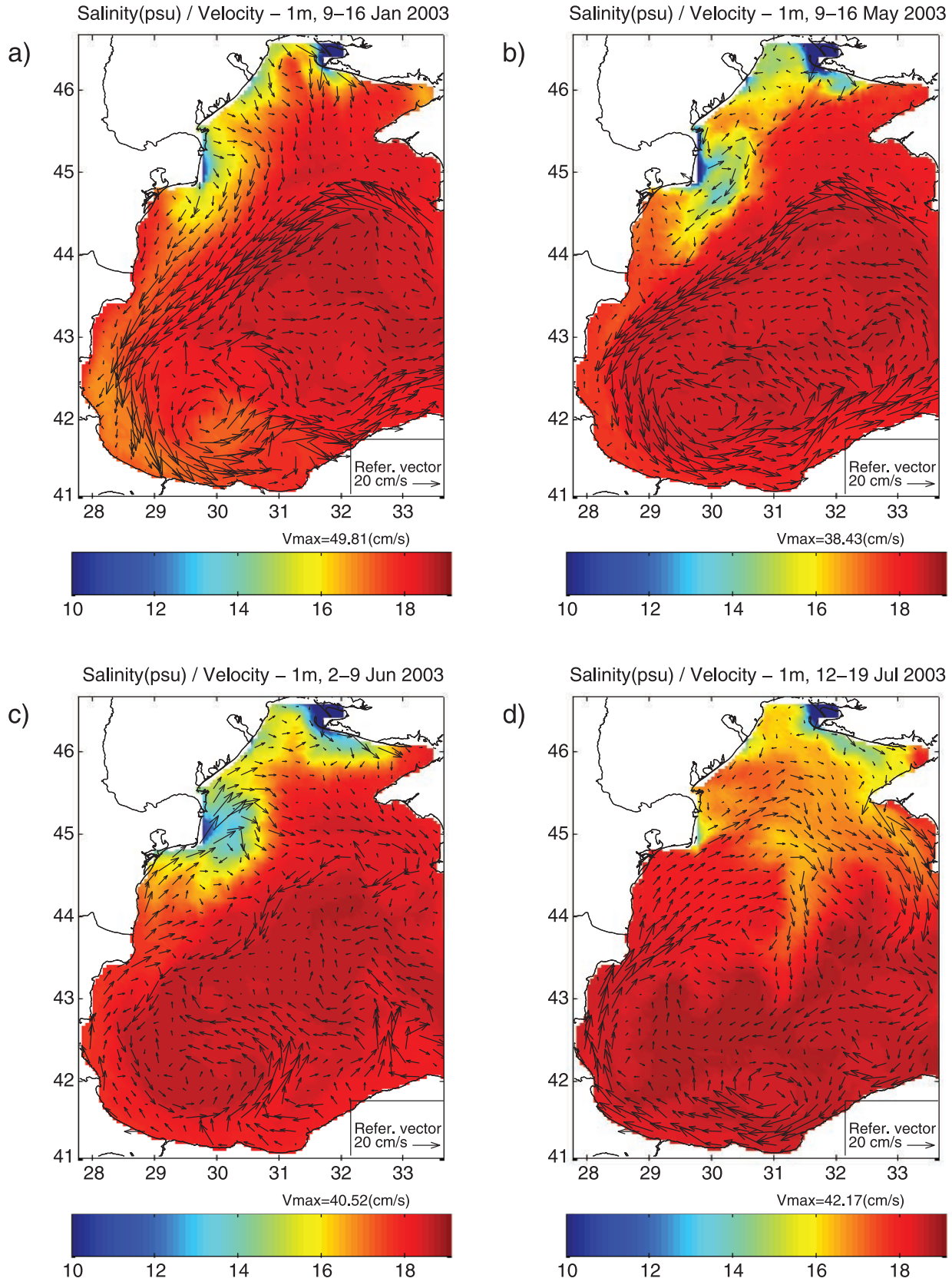

Figure 5. Model simulated near surface fields of salinity and current velocity for weekly averages during 2003 (a) 9–16 January; (b) 9–16 May; (c) 2–9 June; (d) 12–19 July.

waters toward the north and central parts of the Northwestern shelf, while maintaining the anticyclonic turn of the plume bulge. This tendency is particularly evident in the summer months, as shown in Figure 5d, where the plume influenced area has taken over the entire shelf, the spreading supported by the absence of the Rim Current. The weak river discharge and the northward winds have reversed the southward coastal flow along the narrow western shelf that prevailed in the winter months. A cross-shore, north to south pressure gradient develops, as low salinity waters accumulate along the northern coast; this, together with the anticyclonic tendency of the river plume bulge and wind driven currents along the Crimea peninsula, create the pronounced flows across the shelf break and toward the basin interior observed in Figure 5d. The offshore detachment of the plume waters is maintained by the eastward component of the wind stress in July (Figure 3).

[40] We should note that despite the deep topography cutoff (flat bottom at 500 m) that was employed in order to increase the vertical resolution in the open Black Sea area, the substantial bathymetric gradient that is still present across the shelf break, sustains a strong rim current (Figures 5a and 5b) that is similar to the one simulated by the hydrodynamic model with realistic deep bathymetry.

4.2. Seasonal Variability of Phytoplankton Growth

[41] We first examine the seasonal variability of the phytoplankton growth rate as an average for the open sea (deepest area over the 500 m flat bottom depth) and the coastal Danube influenced area (defined as bounded by the 17 psu isohaline, which is the boundary of the front created by the riverine low salinity waters, Figure 5). In the next section, we will discuss the simulated horizontal patterns in comparison with SeaWiFS images for the same periods in 2003.

[42] The phytoplankton concentration that is captured by the SeaWiFS images may be assumed to be representative of the relatively homogeneous zone that is actively mixed from the surface, due to wind stirring and convective overturning in winter. The so-called [*Gregoire et al.*, 2004] "MiXing Layer" Depth (MXLD) depends on the mixing conditions, represented in the model by the vertical eddy diffusivity. For the purposes of our analysis, we define the bottom of the MXLD at the depth where the eddy diffusivity reduces to 10 cm^2/s.

[43] The MXLD variability averaged over the open sea and over the coastal river influenced waters is shown in Figure 6 together with the total attenuation coefficient k_{tot}, the ISM concentration, the phytoplankton growth rate, as well as the light and nutrient limitation functions as averages over the MXLD, again for the open sea and coastal areas. Along with the open sea MXLD variability we have also plotted the one for the critical depth, which is defined as the depth where the integrated phytoplankton growth balances its losses, following *Sverdrup* [1953]. For the total attenuation coefficient, our formulation, which includes an ISM contribution and has used the parameters (k_w = 0.04; k_c = 0.03), is plotted against the formulation by *Oguz et al.* [1996], which does not include ISM and has values (k_w = 0.08; k_c = 0.07).

[44] During winter, the primary production is mostly limited by light availability, due to the reduced incoming solar radiation and the increased vertical mixing. The light limitation in the open sea area (Figure 6a) is as expected stronger than in coastal waters (Figure 6b) due to the higher MXLD (reaching 40–50 m during the stronger wind periods in December and February, Figure 6c; see also Figure 3b). In coastal waters shallow depths and stratification induced by low salinity limit the MXLD to 5–10 m (Figure 6d) and light limitation is mostly due to the increased particulate matter concentrations as a result of resuspension from the sediment and increased river loads. The peaks on k_{tot} for coastal waters (reaching $\sim$1 m^{-1}, Figure 6f) coincide with storm events during December and February, which result in significant resuspension from the sediment (Figure 6h). An increase of k_{tot} in the open sea (Figure 6e) is also observed in correlation with increased suspended matter concentrations (Figure 6g) that slowly decrease after spring, as ISM supply from river load and coastal erosion is diminishing. While the open sea k_{tot} is roughly the same as the one calculated using the *Oguz et al.* [1996] formulation (with differences not exceeding $\sim$0.015 m^{-1}), the differences are noticeable in the coastal areas. The *Oguz et al.* [1996] formulation produces lower light attenuation values during winter, since the particulate matter contribution is not represented, and slightly higher values during summer, which arise from assigning a higher value to the phytoplankton contribution k_c. The simulated k_{tot} values using either formulation were in agreement with available coastal secchi disk observations in the spring to autumn seasons 2002 (A. Cociasu, personal communication). Unfortunately, no observations were available during winter that would permit us to confirm the much higher simulated attenuation coefficient values. However, our representation of the resuspension processes and the correlation with the winter storm events is encouraging and will allow a more realistic parameterization of the light attenuation variability once data become available.

[45] In the beginning of March, the mixing layer depth significantly decreases both in coastal and open sea areas (Figures 6c and 6d), as winds get weaker (Figure 3) and the seasonal thermocline begins to develop. In response, the light limitation function is sharply increased. As soon as the MXLD becomes lower than the euphotic depth, a spring bloom is stimulated, which is marked by the intercept of the mixing layer depth with the critical depth. A more moderate increase is however encountered in phytoplankton growth rate (Figures 6i and 6j) due to the low temperatures in both coastal and open sea areas. In order to investigate the effect of temperature on phytoplankton growth, we have calculated the average growth rate assuming no temperature dependence (i.e., Q10 = 1 in Figures 6i and 6j). The result is a much stronger spring bloom. One should also notice that, surprisingly, a higher impact of temperature in both coastal and open sea areas is observed during the spring period (March–May) rather than the colder, on average, winter period (December–February); lowest temperatures are observed in mid-February for the coastal area and mid-March for the open sea. This is because during the lowest available light period in winter, the phytoplankton growth rate lies in

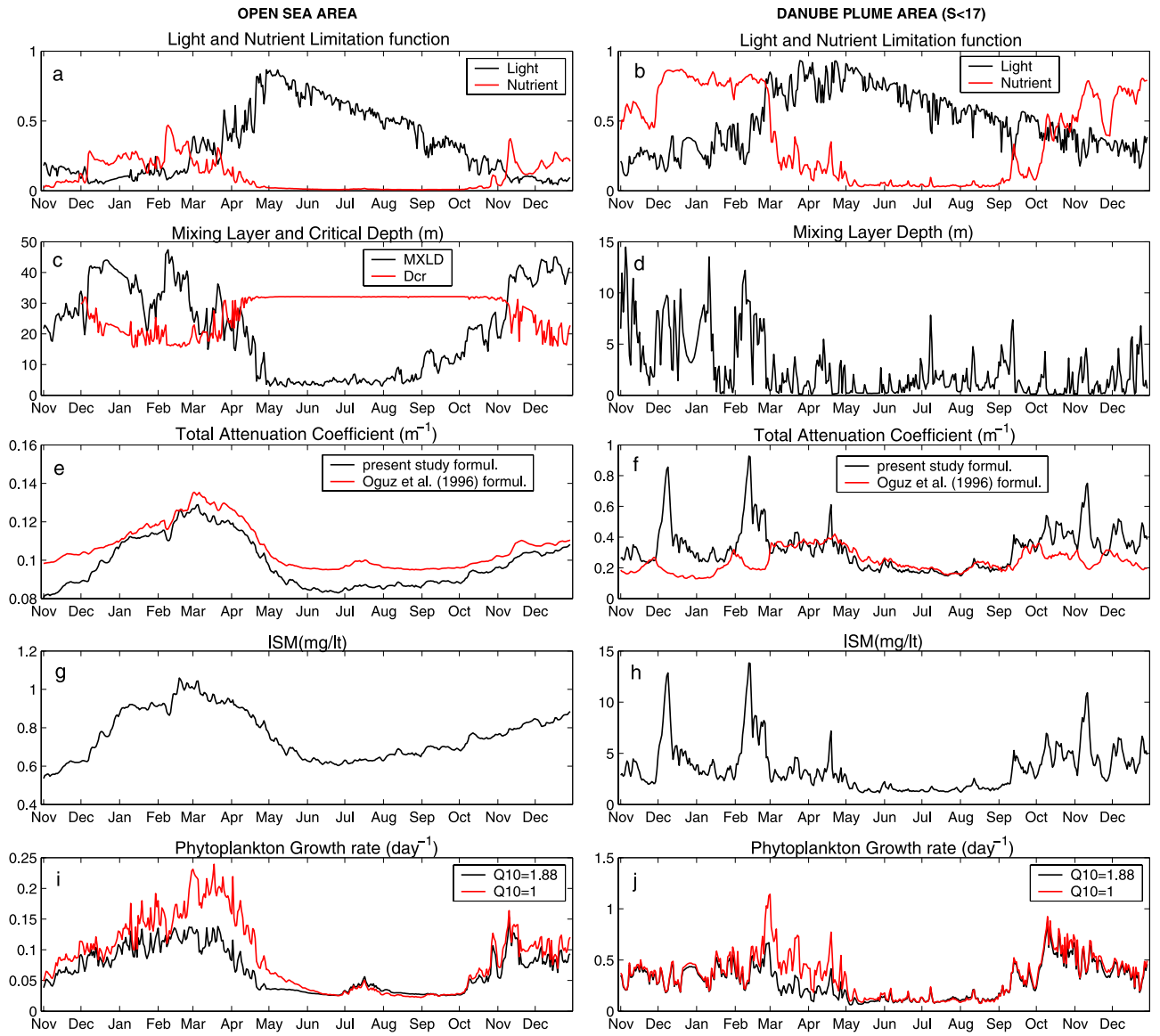

Figure 6. Open sea (left) area and Danube river plume (*SSS* < 17 psu) (right) averages of: (a), (b) light (black line) and nutrient (red line) limitation functions (1 signifies no limitation); (c), (d) the MiXing Layer Depth (MXLD, black line) and Critical Depth (Dcr, red line), (m); (e), (f) total attenuation coefficient formulated in the present study (black line) and as by *Oguz et al.* [1996, red line] (m^{-1}); (g), (h) ISM concentration (mg/lt), (i), (j) phytoplankton growth rate using temperature dependence Q10 = 1.88 (black line) or no dependence Q10 = 1 (red line), (day^{-1}), vertically averaged over the mixing layer depth (defined as the depth where the diffusivity coefficient reduces to 10 cm^2/s).

the beginning of the light limitation curve (also known as the P-I curve), where the variation of the maximum growth rate $P_{max} = \sigma_m L_T(T)$ with temperature has a minor effect, since the photosynthesis efficiency parameter a (representing the initial slope of the P-I curve) is assumed constant. As the light limitation function increases during spring, the impact of the variation of P_{max} with temperature is much higher.

[46] In the open sea area, the late winter-spring bloom is fueled by the nitrates (as nitrogen is the most limiting nutrient) that were brought to the surface from the subsurface deposit during winter and particularly in the December and February stronger mixing periods. As the nitrates are gradually exhausted (not shown), the growth rate (Figure 6i) drops to very low values after May. The vertical mixing increases again after October (Figure 6c) giving rise to an autumn bloom (Figures 6a and 6i). In the river influenced area the nutrient limitation function (Figure 6b) and the associated growth rate (Figure 6j) sharply decrease after the first bloom in the beginning of March. The increase of nutrient river load (Figure 4) and the enhancement of vertical mixing in the autumn period can be accounted for the respective increase of the phytoplankton growth rate.

[47] In Figure 7 we present the model simulated vertical structure of the phytoplankton and zooplankton biomass seasonal variability, averaged over the open sea area. A subsurface chlorophyll maximum (~0.6 mmol N/m^3 which is ~1.2 mg Chl-a/m^3) is simulated during summer at a depth

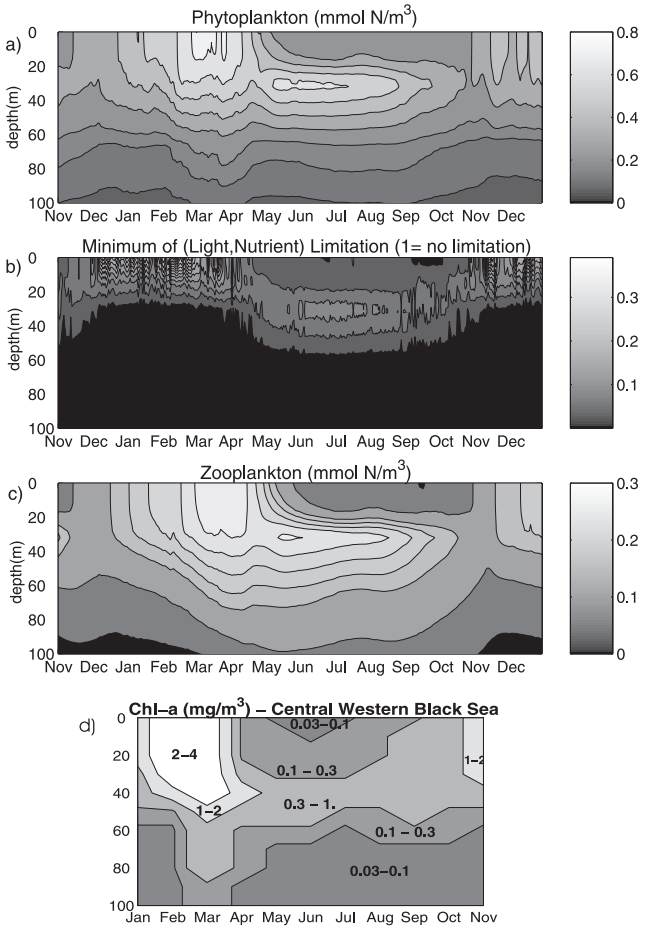

Figure 7. Vertical profile of model computed seasonal variability for (a) Phytoplankton (mmol N/m^3), (b) the minimum of the light and nutrient limitation function (1 signifies no limitation), (c) zooplankton (mmol N/m^3), averaged over the open sea area. The Chl-a (mg/m^3) average vertical profile of seasonal variability in the Western open sea area (data from 1978–1992, redrawn from *Vedernikov and Demidov* [1997]) is shown in (d).

of 30–35 m (Figure 7a) where available light is combined with nutrients diffused from below (Figure 7b). The simulated subsurface Chl-a maximum agrees reasonably well with observations from the 1978–1992 periods [*Vedernikov and Demidov*, 1997, Figure 7d] that reveal a subsurface maximum of 0.6–1.2 mg/m^3 at 30–40 m depth. The model simulated annual mean integrated primary production (141 mgC/m^2/day, assuming a 8.5 C/N ratio) [*Karl and Knauer*, 1991] is about half the one based on observations (367 mg C/m^2/day) during the more eutrophic period 1978–1992. The loss of sinking PON below the euphotic layer ($\sim$60 m) is simulated to about 20% (100 mmol N/m^2/a) of the primary production within the euphotic layer, which agrees well with *Karl and Knauer* [1991] sediment traps measurements (25%). The zooplankton biomass (Figure 7c) follows the phytoplankton biomass variation attaining maximum values of $\sim$0.3 mmol N/m^3 during the spring of 2003.

4.3. Comparison With SeaWiFS

[48] SeaWiFS has a spatial resolution of about 1.1 km at nadir and records images from the Black Sea between 09:00 and 11:00 GMT (11:00 and 13:00 local time) once per day. The ocean color Level-1A data were obtained from the Ocean Color web link of the Goddard Space Flight Center at NASA (http://oceancolor.gsfc.nasa.gov/; also see *Feldman and McClain* [2006]). 169 SeaWiFS full-resolution, daily images for the year 2003 have been processed and analyzed herein for the determination of satellite derived chlorophyll-a concentration (Chl-a mg m^{-3}). The SeaWiFS Data Analysis Software (SeaDAS) [*Fu et al.*, 1998] version 4.8 with MSL12 version 5.2 was used; post-processing in MATLAB was needed to employ the same color scale as for the model results. The Chl-a was calculated with the maximum band ratio (OC4v4) algorithm, as described by *O'Reilly et al.* [2000]. Daily composite images were created when more than one scene for a single day was available. The 8-day mean value was calculated from all existing daily images for the corresponding period.

[49] In Figure 8 we show the model simulated surface phytoplankton patterns against the SeaWiFS Chl-a images for the same time periods covering the entire year 2003. Conversion from nitrogen model units to Chl-a units was made assuming the Redfield ratio C/N = 6.625 and C/Chl-a = 40 [*Ragueneau et al.*, 2002], giving a factor of $\sim$2 (mg Chl-a/mmol N).

[50] The spatial and temporal coverage of the satellite images provided a valuable tool for the evaluation of model results. As seen in Figure 8, there is an overall very good agreement on the horizontal chlorophyll patterns, over different periods in the simulation during 2003. Both computed and observed horizontal patterns are closely linked to the transport pathways of the Danube inputs that were discussed in the previous section.

[51] During winter, phytoplankton growth is limited by light availability in both coastal and open sea areas, as mentioned above. Within coastal areas, both model simulated patterns and SeaWiFS images in January 2003 (Figures 8a and 8b) present a relatively low phytoplankton concentration (as compared to the summer season), which can be attributed to the reduced incoming short wave radiation (minimized in early January 2003, not shown) combined to the increased vertical mixing (Figure 6d) and high light attenuation due to increased ISM concentration. In the river plume area average time series shown in Figure 6, light attenuation and ISM concentration do not present particularly high values in January 2003 because they are mostly correlated to water column depth, while the low-salinity plume (that defines the averaging area) is extended offshore due to occasional westerly winds (Figure 3a). In December and February periods, as the river plume is confined near the coast due to strong northerly winds (Figure 3a), light attenuation and ISM concentration present particularly high values. The model simulated Chl-a is slightly underestimated in the south-western coastal area, following an overestimation of the ISM concentration. We note that model bathymetry over the Bulgarian and Turkish shelf areas is somewhat deeper than in reality due to model smoothing toward the much deeper open sea areas; this can influence the coastal simulated Chl-a. In the northwestern coastal areas, shallow water column depths result in a lower light limitation despite the even higher ISM concentrations. The latter underestimation of phytoplankton within coastal areas

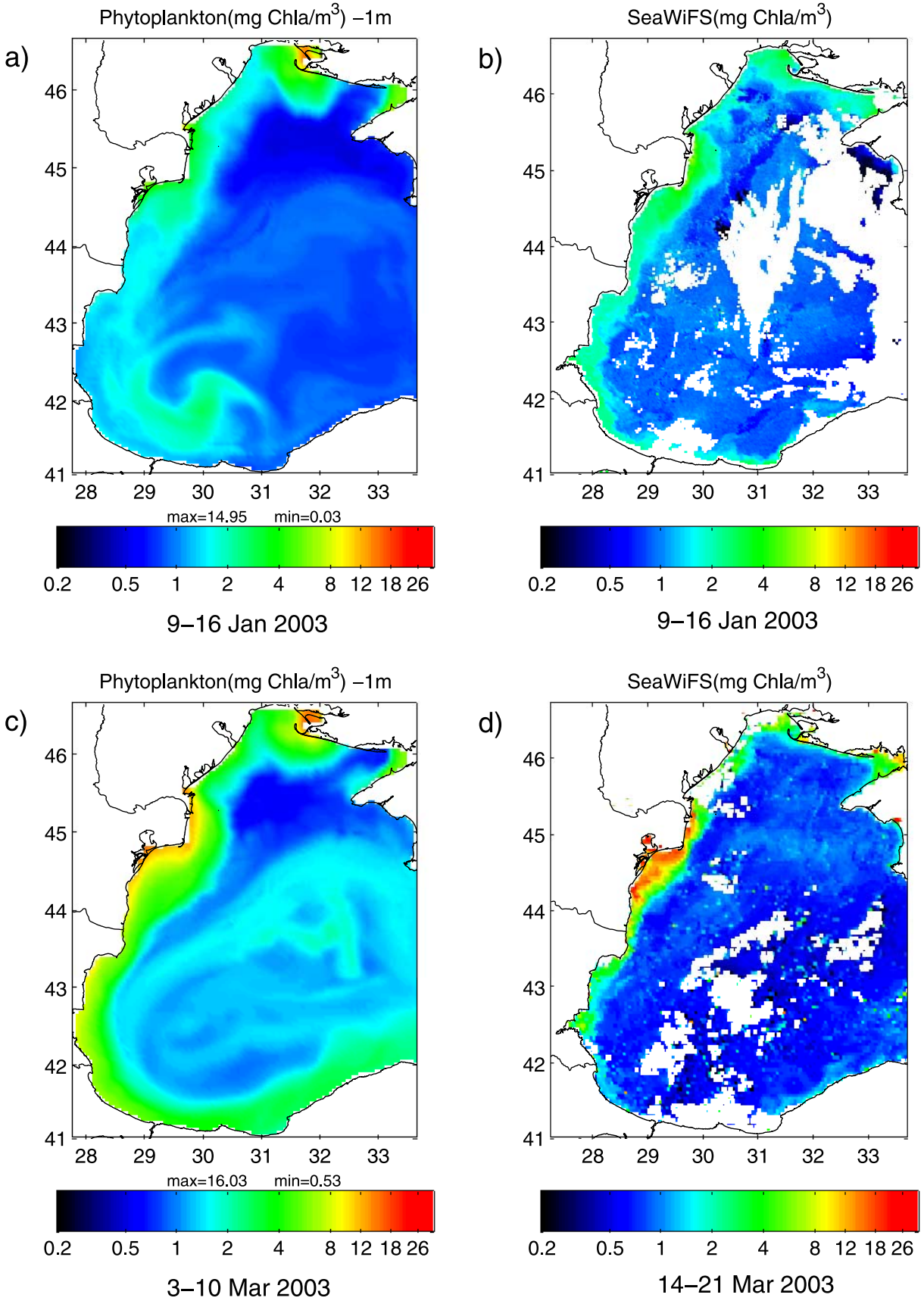

Figure 8a. Model simulated (left) and SeaWiFS (right) chlorophyll-a (mg/m^3) 8-day averages (2003) for (a, b) 9–16 January, (c) 3–10 March, (d)14–21 March.

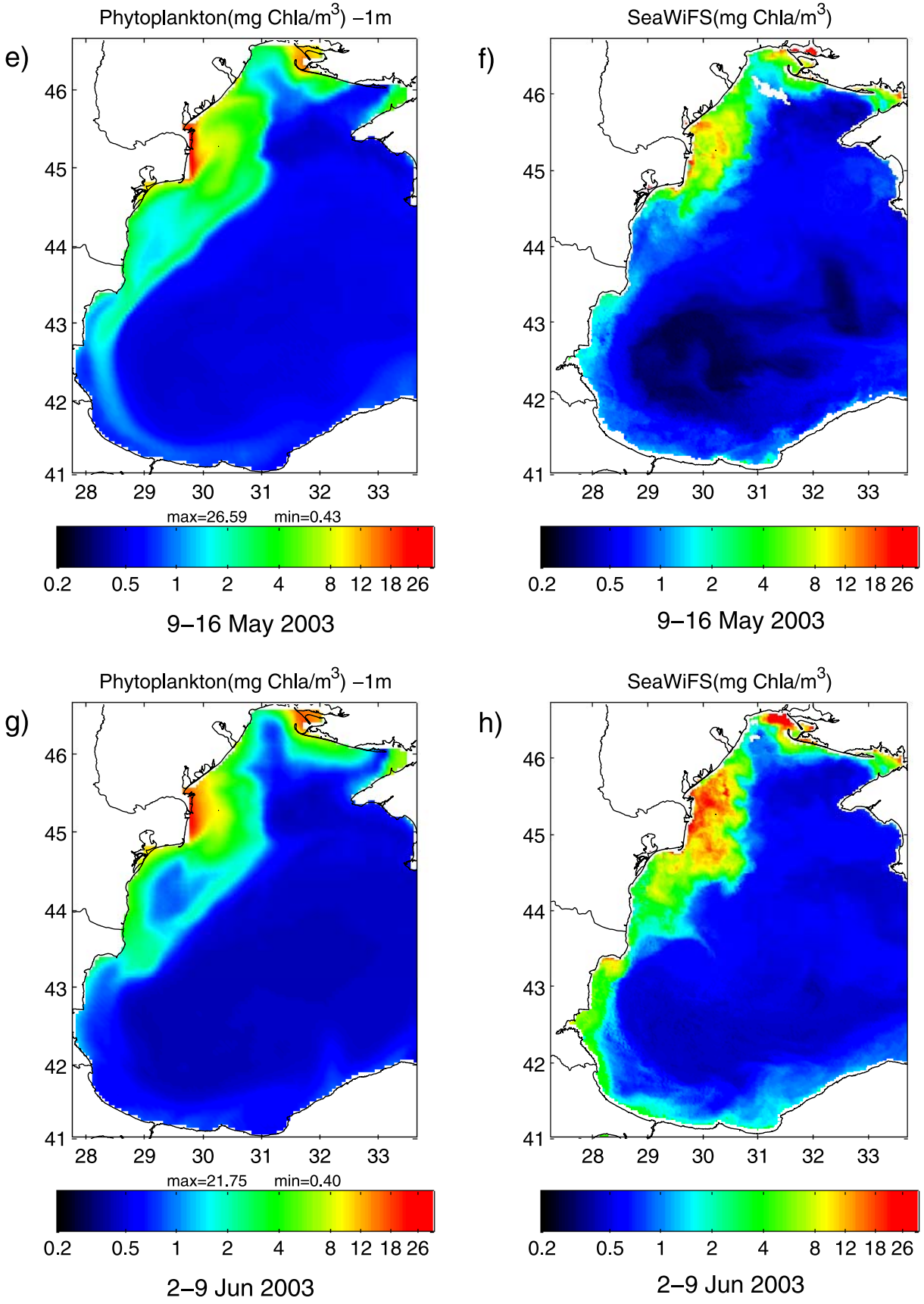

Figure 8b. Model simulated (left) and SeaWiFS (right) Chlorophyll-a (mg/m^3) 8-day averages (2003) for (e, f) 9–16 May, (g, h) 2–9 June.

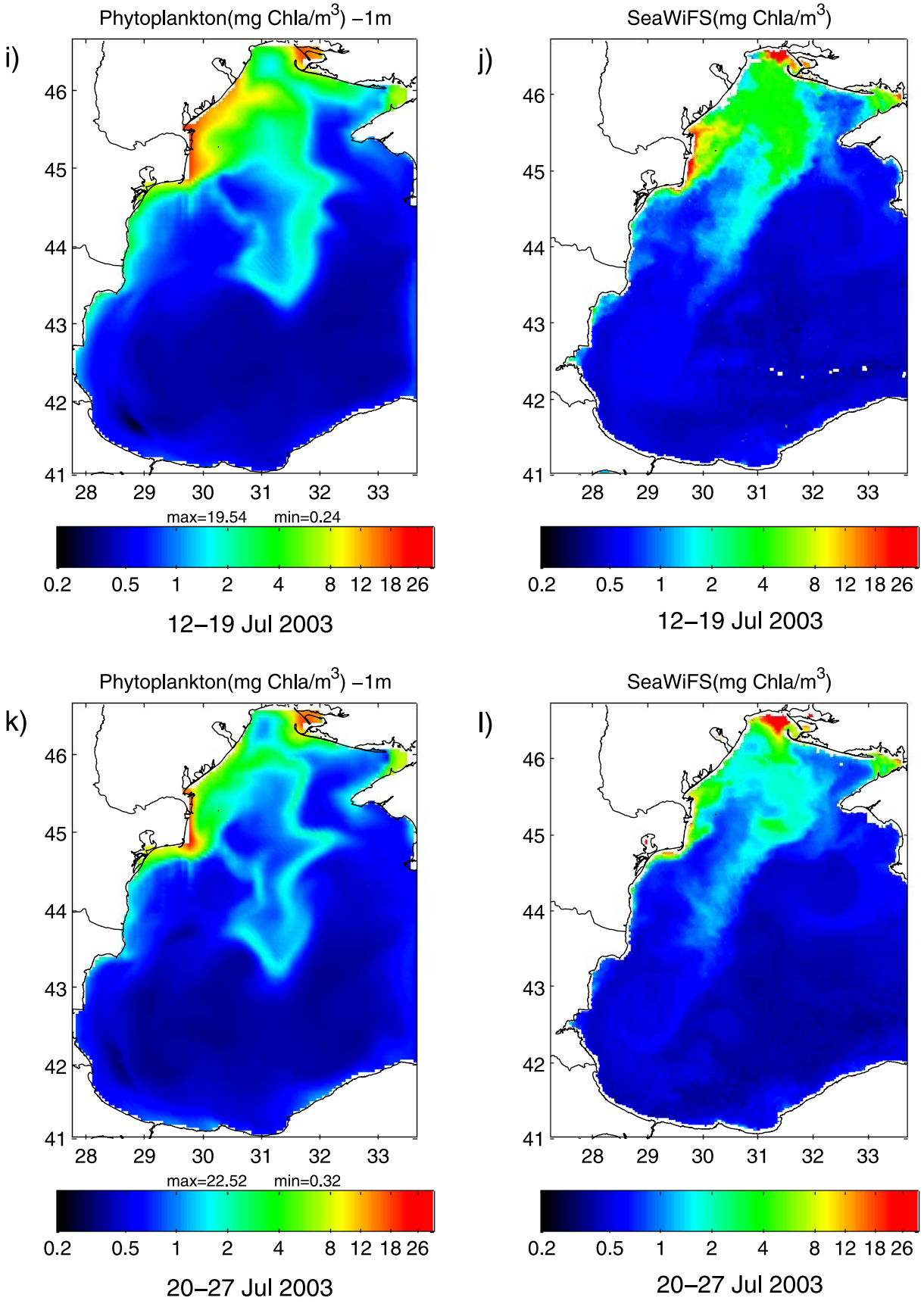

Figure 8c. Model simulated (left) and SeaWiFS (right) Chlorophyll-a (mg/m^3) 8-day averages (2003) for (i, j) 12–19 July, (k, l) 20–27 July.

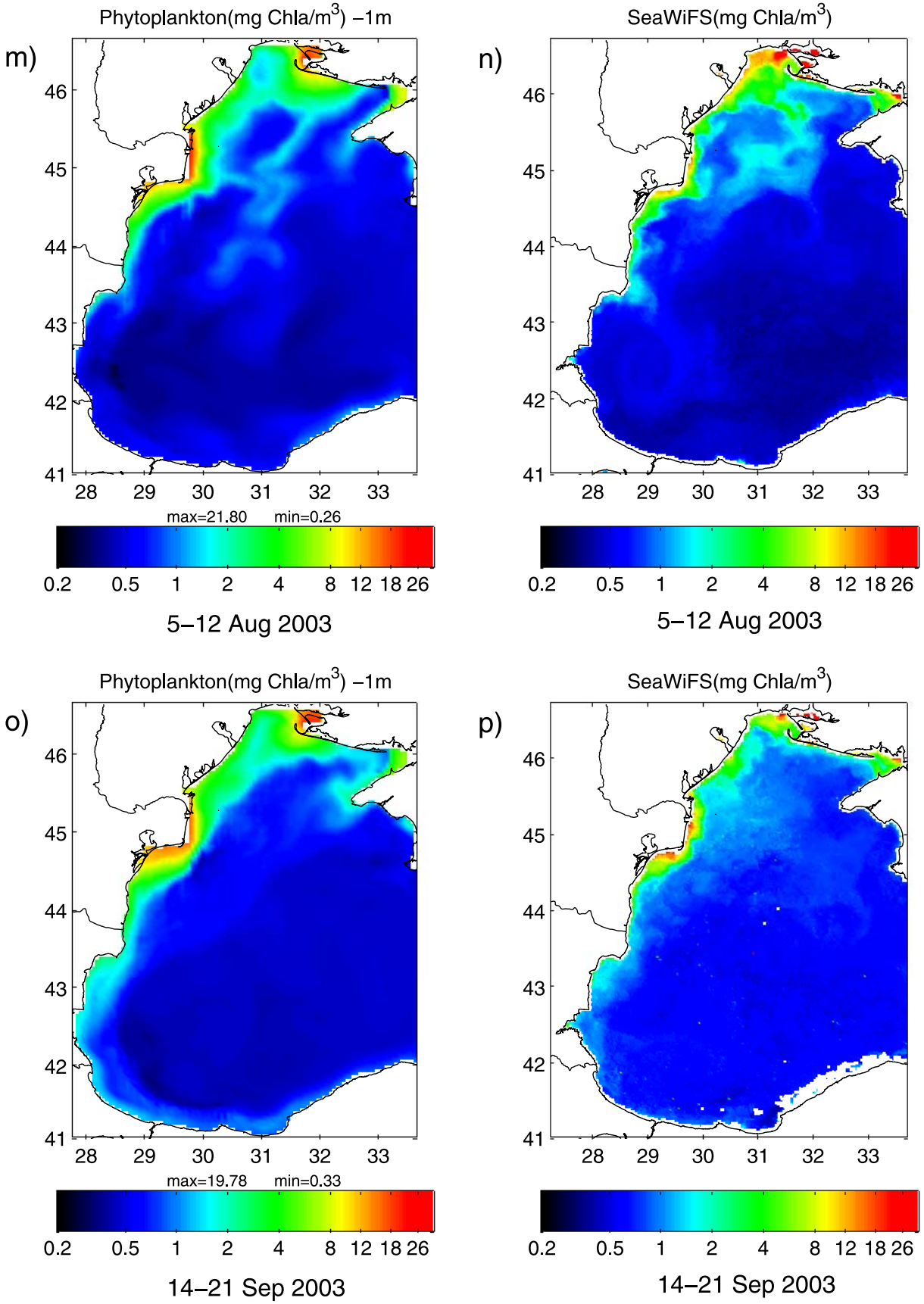

Figure 8d. Model simulated (left) and SeaWiFS (right) Chlorophyll-a (mg/m^3) 8-day averages (2003) for (m, n) 5–12 August, (o, p) 14–21 September.

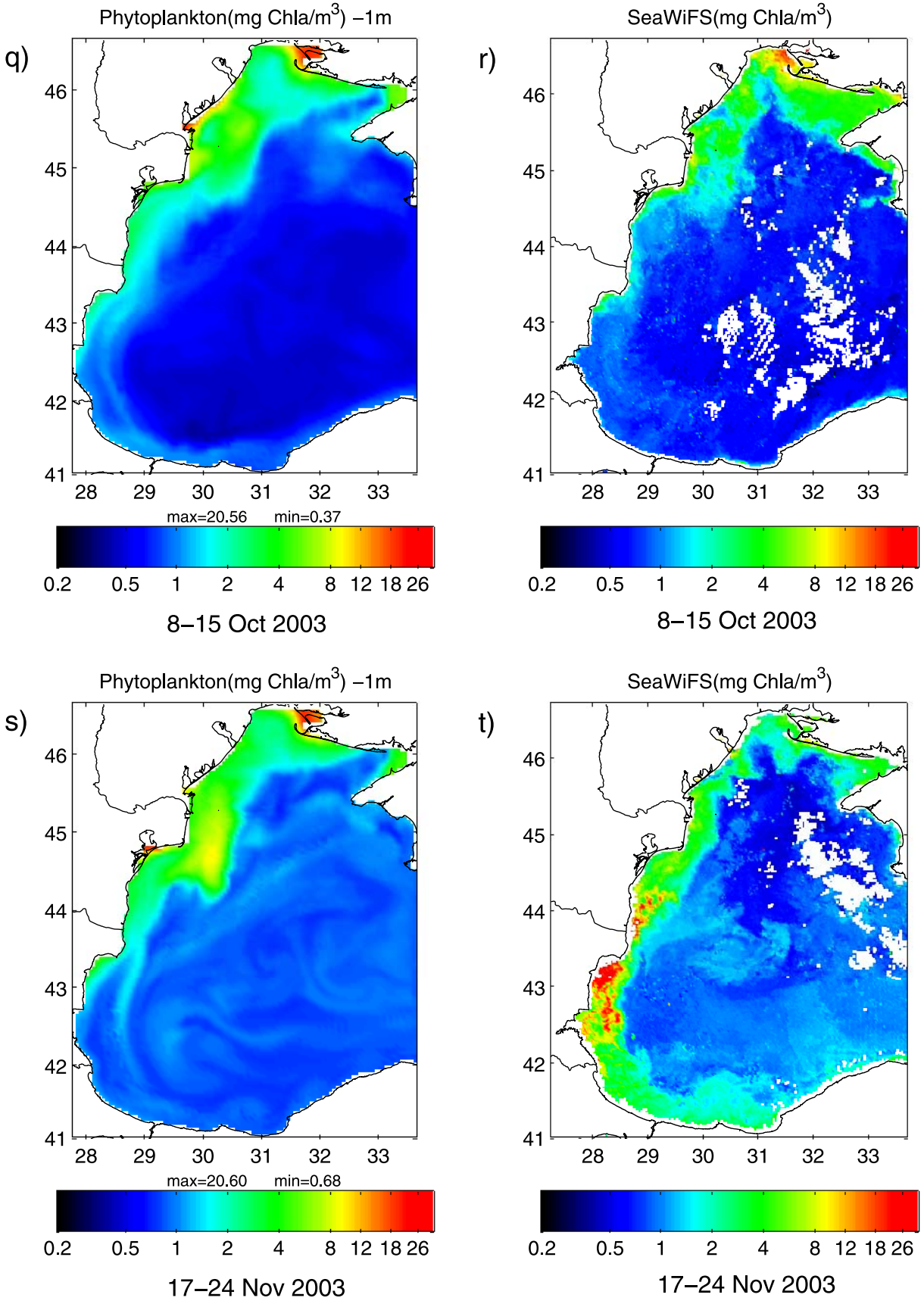

Figure 8e. Model simulated (left) and SeaWiFS (right) Chlorophyll-a (mg/m^3) 8-day averages (2003) for (q, r) 8–15 October and (s, t) 17–24 November.

results in the ''escape'' of nutrients farther offshore leading to a model calculated patch of low-salinity and high-chlorophyll water at around (30°E, 42°N), that is related to a transient cyclonic eddy (Figure 5a). Such frontal eddies are known to be a transport mechanism for high chlorophyll/low salinity waters of coastal origin. Eddies in this area associated with the Rim Current and local topography have been discussed by *Korotaev et al.* [2003]. The timing of this eddy is not confirmed based on the SeaWiFS data. However, transient eddies are obviously extremely hard to be captured by model simulations without data assimilation.

[52] A phytoplankton bloom within the Danube front area and the North Romanian shelf is observed in the SeaWiFS image of 14–21 March (Figure 8d). As there was no available image for early March, we cannot identify the exact bloom initiation period. A similar, although weaker, bloom is simulated by the model slightly earlier in 3–10 March (Figure 8c), as phosphorus is later on quickly exhausted (see nutrient limitation in Figure 6b) leading to a higher underestimation of phytoplankton concentration (as compared with the SeaWiFS image of 14–21 March 2003). This could be attributed to an underestimation of the phosphorus river load or a higher N/P stoichiometry for phytoplankton that would reduce its phosphorus demand (see sensitivity studies discussion). The simulated phytoplankton concentration along the Turkish coast is overestimated as compared to the SeaWiFS image probably due to an overestimation of the nitrogen river load during winter since open sea phosphorus, along the southern Turkish coast, is always not limiting. The model simulated phytoplankton in the open sea area ($\sim$1.5 mg Chl-a/m^3) is higher than in the SeaWiFS image ($\sim$0.8 mg Chl-a/m^3). The most probable reason is the insufficient model vertical resolution (see sensitivity tests discussion) that results in excessive vertical mixing from the subsurface nutrient pool, particularly in areas of sharp bathymetric variation (which coincide with the areas of higher phytoplankton concentration).

[53] During summer, primary production is mostly sustained by riverine nutrients and regeneration processes and thus is confined to river influenced waters and coastal areas, where nutrient fluxes from the sediment provide an additional source. During most of the summer period winds are southerly or southeasterly in the Danube area, thus leading the Danube plume toward the North, Northeast. As the river supply is cut off, the productivity along the Romanian shelf gradually decreases from May until July. Along the Turkish coast, the primary production is occasionally enhanced due to upwelling [*Oguz et al.*, 2002]. Such an enhancement is observed during June (Figure 8h), as winds are easterly (upwelling favorable) there. The model simulated phytoplankton is underestimated along the Turkish coast even though coastal upwelling can be tracked from the simulated temperature patterns (not shown). In fact the simulated Chl-a concentrations are comparable to SeaWiFS at a depth of $\sim$15 m which may be an indication of the fact that the SeaWiFS image is representing an integrated part of the water column according to its light attenuation properties. The Chl-a concentration is slightly higher as compared to the SeaWiFS image, in the coastal area between the rivers Dniestr and Danube in mid July 2003. However, the overall agreement is remarkable, for both coastal and open sea areas.

[54] During the summer nutrient limited period, the high-chlorophyll waters follow the hydrodynamic transport pathways of the Danube plume (also discussed in the previous section) that are greatly influenced by seasonal and higher frequency changes in the wind variability (Figure 3). After a period of persistent southerlies during June 2003 (Figure 3a), the plume, that was spread to the East and Northeast (Figures 8e, 8f, 8g, and 8h), is subjected to an extended anticyclonic turn offshore and to the South, which is augmented by the eastward component of the wind stress (Figures 8i and 8j, see also Figure 5d and related discussion of hydrodynamic patterns). Subsequently, in late July and in the beginning of August, as the winds change to northerlies, the chlorophyll plume that was widely spread over the Ukrainian shelf gradually diminishes (Figures 8k, 8l, 8m, and 8n) due to the cut of supply from the Danube.

[55] During autumn, the onset of cold fronts and northerly winds elongated the plume along the western Black Sea coast (Figures 8o and 8p). As the increased wind stirring enhances the resuspension of organic matter from the sediments and the vertical diffusion from the subsurface nutrient pool, primary production is increased over the shelf and open sea areas. The simulated autumn bloom in the open sea area is not as strong, as compared to SeaWiFS, and shifted toward November probably due to an underestimation of vertical mixing (see sensitivity studies discussion). Another possible cause for the observed more intense autumn bloom could be an increased higher predator zooplankton mortality, as suggested by *Oguz et al.* [2002]. In the river influenced waters a decrease of Chl-a is revealed by both model simulated and SeaWiFS October and November 2003 patterns, which can be attributed to the light limitation related to increased ISM concentration (Figures 6f and 6h). The underestimation of model simulated Chl-a for November 2003 in the western coastal areas most likely arises from the inaccurate simulation of ISM, similar to the January 2003 results that were mentioned above.

[56] In Figure 9, we show the average model simulated surface Chl-a variability against the SeaWiFS one, within the extended Danube influenced area (shown in Figure 1 as area D) and over the open sea. In the Danube area, which is characterized by a high spatial variability, the model simulated average Chl-a is slightly elevated as compared to the SeaWiFS, owing mostly to the greater extension of the high Chl-a plume and generally the relatively smoother model fields that mask the sharp gradients across the front. This is to a certain point expected due to model limitations imposed by the horizontal resolution, as well as to the probably excessive horizontal diffusion that is adopted as a remedy to numerical noise and which would be minimized when shifting to a finer resolution model. A reasonably good correlation between model and SeaWiFS Chl-a variability can be noted except for the SeaWiFS Chl-a peak in the beginning of June that is related to a much more extended plume, observed also in the 2-D patterns (Figures 8g and 8h). The open sea area, model simulated Chl-a overestimation during spring and underestimation during autumn that was discussed above, can be seen in Figure 9b. During summer, the open sea area model Chl-a levels are rather similar to those of SeaWiFS. The annual average RMS difference between model and SeaWiFS Chl-a within the Danube and open sea areas were 0.43 mg/m^3 and 0.27 mg/m^3 respectively.

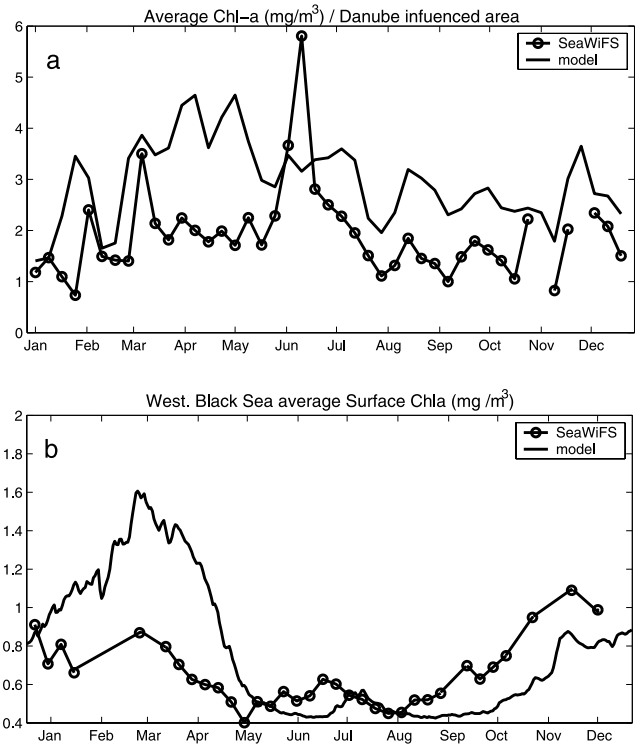

Figure 9. Average surface Chl-a(mg/m^3) as simulated by the model (solid line) and from the SeaWiFS 8-day images (line with circles) for (a) the extended Danube influenced area (shown in Figure 1 as area D) and (b) the open sea area.

[57] In the above discussion we attempted to evaluate the model simulated Chl-a patterns employing SeaWiFS images that offered good spatial and temporal coverage. However, we should note that satellite derived Chlorophyll-a patterns are subject to certain accuracy limitations, resulting from sensor capabilities, calibration procedures, choice of bio-optical algorithms etc. (see *McClain et al.* [2006], for a review on SeaWiFS validation). For this particular application, the OC4v4 algorithm was found to retrieve in situ measured chlorophyll-a concentrations (from 68 stations during 2002 and 2004 in the western Black Sea), in the remote sensed depth, with a mean normalized bias $\left(\frac{1}{n}\sum_{i=1}^{n}\left(\frac{Chl(Sat)_i - Chl(in\ situ)_i}{Chl(in\ situ)_i}\right) * 100\right)$ of 30% and a random error $\left(stdev\left(\frac{Chl(Sat) - Chl(in\ situ)}{Chl(in\ situ)}\right) * 100\right)$ of 77% [A. Davidov, submitted, 2007]. An overestimation of chlorophyll-*a* was found in the open sea area (for Chl-a values <1 mg m^{-3}), by applying the OC4v4 algorithm, mostly due to the high remotely sensed depth extending to the deep chlorophyll maximum during the summer period. An underestimation was found in coastal eutrophic waters (for Chl-a values >10 mg m^{-3}) due to atmospheric correction and bio-optical algorithm limitations. Despite the SeaWiFS data current accuracy limitations, their use in the context of a mostly qualitative comparison with model simulated Chl-a was particularly valuable, providing a better understanding of phytoplankton temporal and spatial variability and permitting a thorough model calibration.

4.4. Benthic Fluxes, N/P Limitation and the Impact of Nutrient Load on the Open Sea Productivity

[58] In Figure 10 we present the seasonal variability of the nitrogen and phosphorus fluxes at the sediment interface that result from resuspension/deposition of organic matter and diffusion of phosphate and ammonium from the sediment. The averaging area is the Danube front area, of about 2400 km^2 (area C in Figure 1), so as to be comparable with the estimates of *Friedrich et al.* [2002, Figure 8]. During winter, the net deposition (deposition minus resuspension) of POM is minimum, since primary production (which is the main source of POM) is reduced due to the light limiting conditions, while the increased vertical mixing enhances resuspension from the sediment and/or prevents the POM deposition. However, a small proportion of the resuspended organic matter is decomposed, as the remineralization rate is a function of temperature and phytoplankton biomass (both reduced during winter). The POM net deposition attains maximum values during summer (May–August), as wind stirring is weak and primary production is high. During short periods of stronger wind stirring, resuspension from the sediment is enhanced, resulting in the nutrient enrichment of surface waters. The variation of the diffusional flux of phosphate and ammonium from the sediment is defined by the temperature seasonal variability, as well as the variability of the sediment pool concentration according to the deposition/resuspension history. The phosphates benthic flux roughly balances net sedimentation, representing an important nutrient source that is comparable to the phosphorus river load, particularly during summer. The adopted benthic fluxes of ammonium and phosphates are characterized by a N/P molar ratio of about 7:1, accounting for the losses of nitrogen through denitrification in the sediment. Therefore, the sediment fluxes are expected to

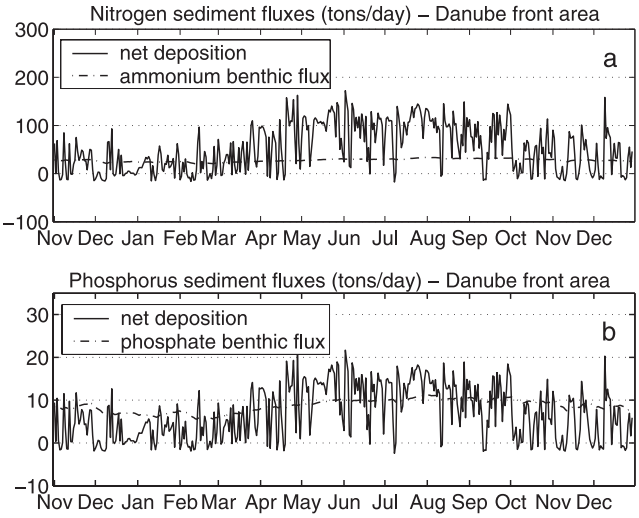

Figure 10. Model computed seasonal variability of (a) nitrogen and (b) phosphorus sediment fluxes (tons/day) in the Danube front area (~2400 km^2, shown as box C in Figure 1). The solid lines represent the net deposition (deposition minus resuspension) of nitrogen and phosphorus parts of detritus respectively for (a) and (b). The dash-dot lines represent the ammonium and phosphate benthic flux respectively for (a) and (b).

Table 4. Model Simulated Annual and Seasonal Nitrogen and Phosphorus Mean Sediment Fluxes in the Danube Front Area (2400 km^2, Shown as Box C in Figure 1), Along With Danube River Loads[a]

	Net Deposition (Tons/Day)		Benthic Flux (Tons/Day)		River Load (Tons/Day)	
Period	Nitrogen (Detritus-N)	Phosphorus (Detritus-P)	Nitrogen (NH4)	Phosphorus (PO4)	Nitrogen (NH4 + NO3)	Phosphorus (PO4)
Winter	12.9	2.2	23.4	6.6	1147	22
Spring	67.7	8.8	26.1 (43)	8.2 (7)	1215	22
Summer	92.1	11.8	30.7 (66)	10.2 (17)	297	11
Autumn	48.1	6.6	29.6	9.5	327	15
Annual	55.3	7.3	27.4	8.6	745	17

[a]Values in parenthesis represent estimates based on measurements during spring 1997 and summer 1995 [*Friedrich et al.*, 2002].

contribute to a nitrogen limitation of primary production in coastal areas that are outside the immediate influence of river inputs.

[59] The annual and seasonal mean benthic fluxes for the Danube front area (Figure 1) are presented in Table 4. The simulated phosphate flux for spring 2003 (8.2 tons/day) is rather close to the estimate of *Friedrich et al.* [2002] for spring 1997 (7 tons/day), while the simulated flux for summer 2003 (10.1 tons/day) is considerably lower than the estimated flux for summer 1995 (17 tons/day). The model simulated ammonium flux was fitted to lower values (26 tons/day for spring and 31 tons/day for summer) than *Friedrich et al.* [2002] estimates (43 tons/day for spring 1997 and 66 tons/day for summer 1995), because adopting a higher ammonium flux was found to produce an overestimation of phytoplankton during the summer to autumn period, mostly along the Ukrainian coastal areas. The simulated ammonium fluxes represent about 49% of the nitrogen net sedimentation, which is similar to the budget calculation (37%) of *Gregoire and Friedrich* [2004] for the 1995/1997 period. Therefore it seems that the simulated decrease of ammonium benthic fluxes, as compared to the 1995–1997 period, is consistent with a similar decrease of nitrogen net sedimentation (model simulated ~3 mmol N/m^2, compared to ~5 mmol N/m^2 from *Gregoire and Friedrich* [2004]). Such a decrease of the net sedimentation rates and subsequently of the phosphate and ammonium fluxes can be attributed to the phosphate river load reduction (~50%) since the 1995/1997 period [*Velikova et al.*, 2005; *Cociacu et al.*, 1997].

[60] In Figure 11 we show the lines where the dissolved inorganic nitrogen to phosphorus ratio at the sea surface equals the Redfield ratio N/P = 16:1, thus setting the boundaries between the N and P limitation areas. During winter (December–February) the P-limitation extends from the Danube area to the Turkish coast, as river loads are characterized by very high N/P ratios. In spring (March–May) the south extent of the P-limitation area is diminished, as the river load N/P ratio is decreasing. It starts to attain a preferred spreading toward the northern Danube area due to the advection of the river plume that results from the southern winds prevailing during May (Figure 3a, 8e, and 8f); this is also evident during the summer period that is dominated by winds from the south and west. During summer and autumn, the extent of the P-limited domain gradually diminishes in the Danube front area as the N river load is greatly reduced (Figure 4), while benthic fluxes (characterized by N/P ratio of ~7:1) also contribute to N-limitation.

[61] A significant amount of riverine nutrients reach the open sea providing an additional source to the open Black Sea productivity that is mostly sustained by the subsurface nitrate pool, which in turn lies in a dynamical balance according to this additional source of nitrogen and the losses through sinking organic matter bellow the suboxic layer. In order to assess the impact of the river (mostly Danube) nutrient loads and fluxes from the coastal sediments to the open sea productivity, we performed a simulation identical to the reference one (Run 1), but setting both the river nutrient inputs and sediment nutrient fluxes to zero (Run NRS). In Figure 12, we show the open sea average integrated primary production and phytoplankton biomass over the euphotic layer for the 2 simulations. The contribution of river nutrient loads and benthic fluxes to the open

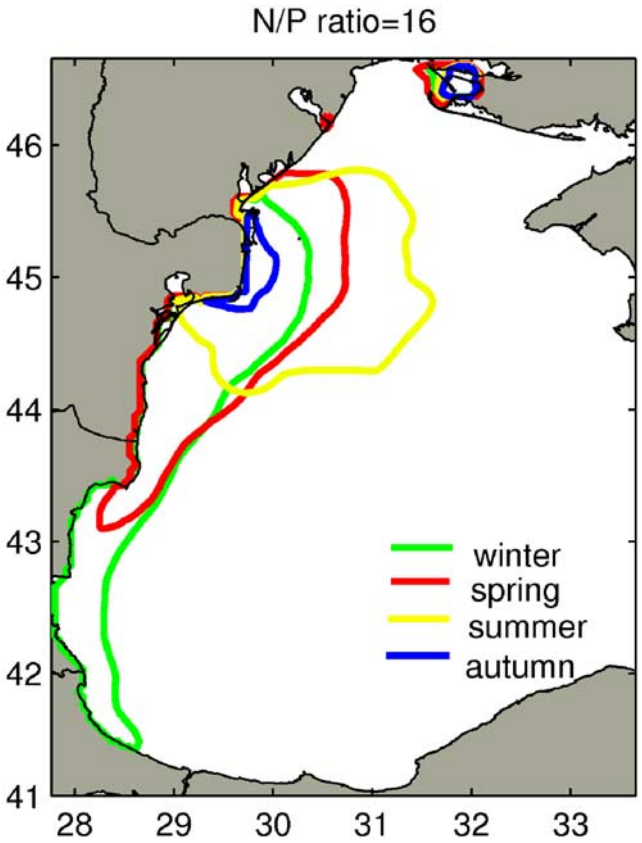

Figure 11. Contours where the model simulated dissolved inorganic N/P molar ratios at the sea surface, equal to 16:1, averaged over seasons.

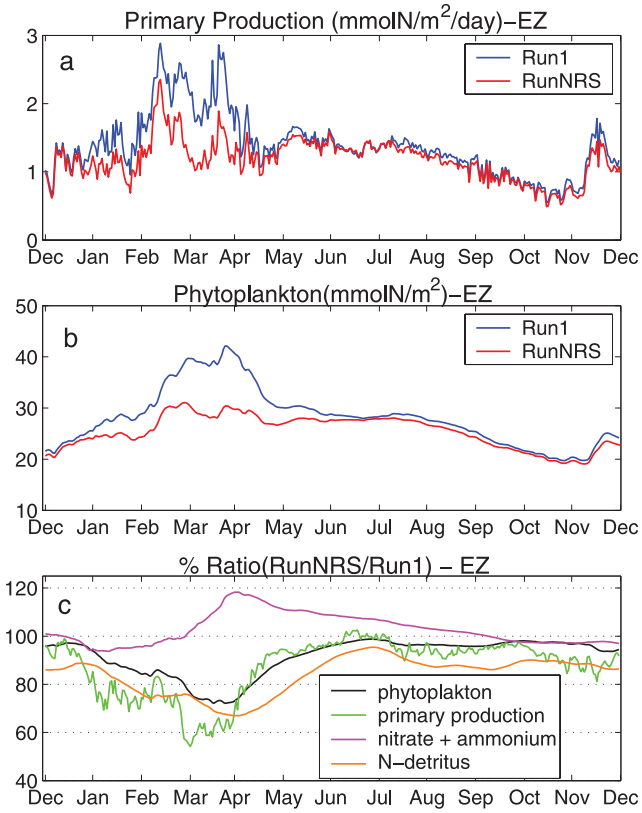

Figure 12. (a) Open sea average primary production (mmolN/m^2/day) over the euphotic layer, for the reference simulation (Run 1, blue line) and the simulation with River nutrient inputs and sediment fluxes eliminated (Run NRS, red line), (b) euphotic layer phytoplankton biomass (mmol N/m^2) for the same runs and (c) Run NRS/Run 1 ratio of simulated phytoplankton biomasses (black line), primary productions (green line), inorganic dissolved nitrogen (magenta line) and N-detritus (orange line).

sea productivity is higher during winter and spring periods as light limitation in coastal waters results in a reduced primary production. Given also the increased river loads during winter, a significant amount of riverine nutrients are not assimilated in coastal waters, thus reaching the open sea area. As shown in Figure 12c that presents the relative ratios between the two simulations (Run NRS/Run 1), the Run NRS primary production decreases up to ~55% of the reference one during March with an annual mean decrease of 82%. The inorganic dissolved nitrogen is lower in the reference simulation (Run NRS/Run 1 > 1) during the spring/summer period as it is assimilated by the significantly higher phytoplankton biomass, but is later compensated by the remineralisation of organic N-detritus (Run NRS/Run 1 < 1) and ends up being 3% higher as compared to Run NRS over the yearly simulation. The integrated total nitrogen (DIN + living and dead organic matter) of the reference simulation ends up 5% higher than Run NRS. Given the short residence time (a few years) of the nitrate inventory [*Konovalov and Murray*, 2001] we would expect a more noticeable impact by the elimination of river inputs in RunNRS. However, this is not surprising, since the model does not resolves the nitrate sharp decrease in the suboxic zone through the denitrification process (a constant value is assigned bellow the maximum) which results in a practically constant subsurface maximum, that actually leads to a 15% increase per year of the nitrate inventory in both simulations.

4.5. Comparison With in situ Data

[62] In Figure 13 we show the model simulated Chl-a, nitrate, phosphate and inorganic suspended matter in the Danube prodelta area and the South Romanian shelf area against in situ data that were collected during 2003 [*Velikova et al.*, 2005; A. Cociasu, unpublished data]. The two averaging areas together with the measurements locations are shown in Figure 1. The significant horizontal variability that all variables exhibit along the productivity gradient makes such a comparison a bit difficult but also beneficial, particularly regarding the dissolved nutrients variability.

[63] In the South Romanian shelf area there is a remarkably good agreement between model simulated and observed Chl-a values during all seasons. Despite this agreement in chlorophyll values, the model simulated nutrient concentrations exhibit certain periods that differ from the observations. Both model results and in situ measurements exhibit a drop in nitrate and phosphate following the early March 2003 spring bloom, but the model phosphate drops too fast, as already mentioned. During May, phosphate, which is the limiting nutrient, is practically depleted. From late June and later on, where nitrogen is the limiting nutrient, the situation reverses and nitrate is depleted. This probably indicates an overestimation of the nutrient uptake rates that results in the diminution of limiting nutrients concentrations. Maximum photosynthesis rate and phytoplankton internal nutrient pools are known to vary depending on the actual nutrient conditions. The explicit simulation of such a variation, however, would require a much more sophisticated phytoplankton growth model with Chl-a as an explicit state variable [e.g., *Geider et al.*, 1998]. In order to prevent the underestimation of the limiting nutrients concentrations, we also tested employing a higher remineralization rate, combined with a higher grazing pressure, so as to maintain the correctly simulated Chl-a variability. While the simulated phosphate (not shown) approached the in situ values, although not as expected for a twice-higher adopted remineralisation rate, the simulated nitrate levels during summer were still much lower. This result might be related to an underestimation of the ammonium benthic flux for this particular area, since adopting an overall higher ammonium flux resulted in a phytoplankton overestimation in the Ukranian coastal areas, as mentioned in the previous section. Further tuning of the remineralization rate would require the addition of bacteria as a model state variable. Bacteria are usually characterized by a higher nitrogen and phosphorus content than phytoplankton [*Goldman et al.*, 1987] and take up main inorganic nutrient forms in order to meet their stoichiometric demands. The net remineralization rate depends on the above stoichiometric differences as well as the organic matter and nutrient availability [*Goldman et al.*, 1987; *Tanguy and Loreau*, 2001; *Fasham et al.*, 1990] and

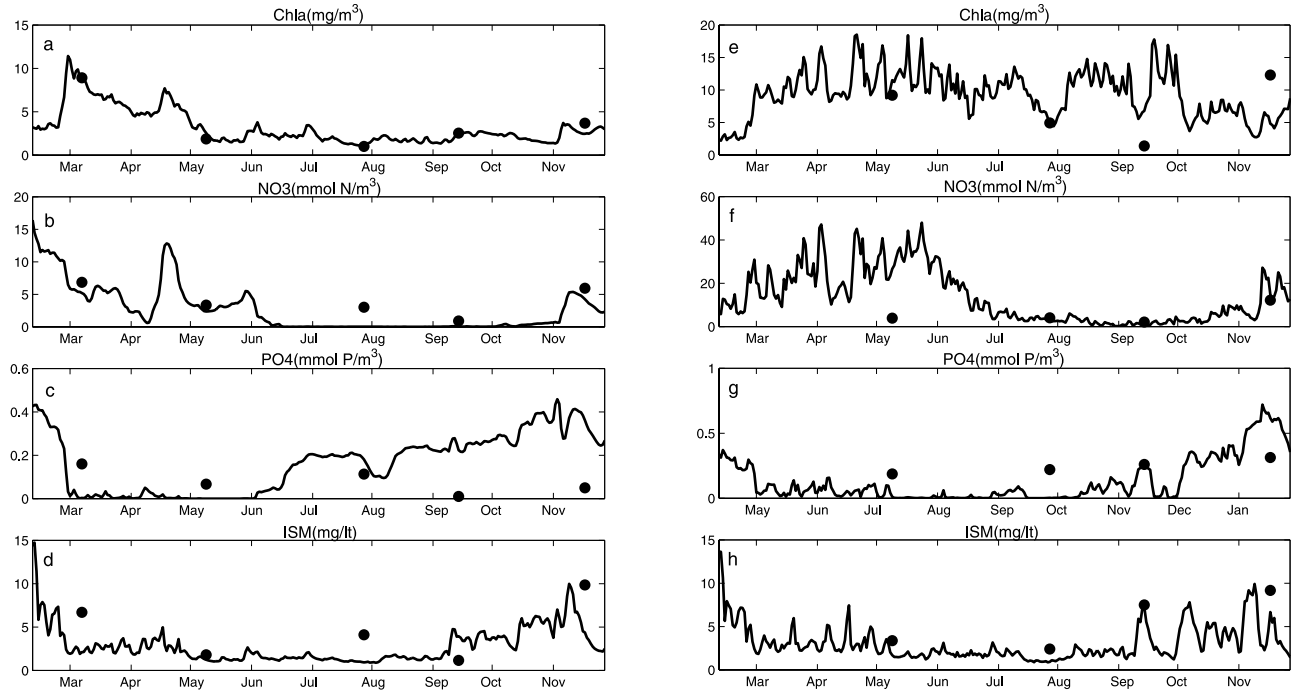

Figure 13. Model simulated (continuous line), from top to bottom: Chlorophyll-a (mg/m^3), nitrates (mmol N/m^3), phosphates (mmol P/m^3) and inorganic suspended matter (mg/lt), against in situ measurements (dots) in (a), (b), (c), (d) averaged over the Danube prodelta area and (e), (f), (g), (h) averaged over the South Romanian shelf area (see area boxes A and B in Figure 1).

therefore its dynamic variability cannot be properly represented by the simplified formulation in the current study.

[64] In the Danube prodelta area, the model simulated Chl-a values agree fairly well with the observed, in May and August 2003. Perhaps an overestimation is suggested by the fact that the observed values lie at the lower limits of the model simulated Chl-a variability. However, some discrepancies would be anticipated in the Danube front area, due to the model uncertainties related to the initial dispersion of the river outflow and also because the effect of low salinity on phytoplankton [*Ragueneau et al.*, 2002] has not been taken into account. In September 2003, in situ Chl-a values are curiously very low (below 1mg/m^3 for most stations) which can be attributed to a short event of diminished river plume that cannot be tracked from the SeaWiFS (or the model simulated) patterns. In November 2003, the model simulated Chl-a is lower than the observed, resulting from the small-scale differences between the model and SeaWiFS Chl-a horizontal distributions (Figures 8s and 8t), which were attributed to an overestimation of the ISM related light limitation. The model simulated nitrate concentration presents a good agreement with the observed values, except in the spring period where the model prediction is too high, probably due to an overestimation of the nitrogen river input during winter, as already mentioned. Phosphate, which represents the limiting nutrient throughout the year, is underestimated in May and particularly in August; a similar reasoning as with the Romanian shelf case applies. In November, higher model simulated phosphate can be attributed to the underestimation of phytoplankton, explained above. The excess of phosphate in the Danube prodelta area also contributes to the overestimation of phosphate that is encountered in the Romanian shelf area.

[65] The model simulated ISM presents a close agreement with observed ISM concentrations in the Danube area, indicating a good quality of the provided ISM river load

Table 5. Biological Parameter Values Adopted by the Different Model Simulations[a]

Simulations	$K_N(P)$	$K_Z(Z)$	$m_z(Z, T)$	K_{mz}	k_s	$R_{N/P}$
Run 1 (Reference)	*0.5 + 0.5 P*	*0.2 + 1.3 Z*	*0.45*	*0.08*	*0.07*	*16*
Run 2	*0.8*	•	•	•	•	•
Run 3	•	*0.5*	*0.04*	*0.1*	•	•
Run 4	•	•	*0.04*	*0.1*	•	•
Run 5	•	•	*0.35*	*0.06*	•	•
Run 6	•	•	*0.35*	•	•	•
Run 7	•	•	•	•	*0.03*	•
Run 8	•	•	•	•	*0.11*	•
Run 9	•	•	•	•		20

[a]The dots indicate a value identical to the reference simulation.

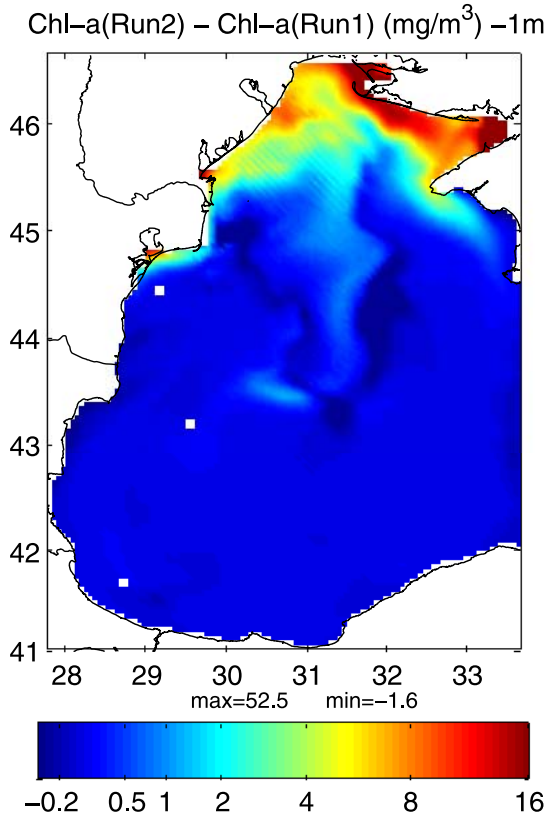

Figure 14. Difference in the simulated Chlorophyll-a (mg/m^3) by Run 2, adopting a half-saturation constant value of K_N = 0.8 (mmol N/m^3) and the reference simulation Run 1, for 12–19 July 2003.

data from the Danube delta model, while a rough agreement is also found in the Romanian shelf area.

4.6. Sensitivity Studies

[66] In this section a series of sensitivity experiments are discussed. First, we explore the impact of ratio-dependent formulations for nutrient uptake and zooplankton grazing. Second, we examine the role of grazing pressure on phytoplankton dynamics in the context of the present study formulation. Finally, we investigate the factors controlling the most important model Chl-a deviations as compared to SeaWiFS data, namely in the open sea area during the spring/autumn periods and in the Danube prodelta area during March 2003. The parameter values for the different simulations are shown in Table 5.

[67] In order to demonstrate the effect of using a variable half-saturation function (rather than constant) for nutrient uptake and zooplankton grazing, we performed two additional simulations using constant values for K_N = 0.8 mmol N/m^3 (Run 2) and K_Z = 0.5 mmol N/m^3 (Run 3), which represent the annual mean values of the adopted varying $K_N = f(P)$ and $K_Z = f(Z)$ functions over the open sea area. Major differences from the reference simulation (Run 1) would thus be expected within coastal/Danube influenced waters that are characterized by much higher values.

[68] In Figure 14 we show the difference in the phytoplankton patterns as simulated by Run 2 and Run 1 during July 2003. An overestimation of phytoplankton concentration is evident for Run 2 in river-influenced waters, particularly in shallow coastal areas. Assigning a constant value of K_N = 0.8 mmol N/m^3, which is much lower than the one assigned by the variable $K_N = f(P)$ in the eutrophic waters (~3 mmol N/m^3 on average), results in increasingly overestimated phytoplankton growth rate across the productivity gradient. In shallow coastal areas this overestimation is particularly high due to the positive feedback between the increased POM sedimentation and the benthic nutrient flux.

[69] Since the grazing pressure in the eutrophic waters is rather low, due to the increased zooplankton mortality induced by higher-predators, the impact of using a different grazing formulation on phytoplankton dynamics would be rather small, as already mentioned. Therefore, in order to reveal the behavioral difference between the Holling formulation and the adopted "ratio-dependent" formulation, the zooplankton mortality rate was decreased to a low level (as for the phytoplankton) and the reference simulation was repeated adopting the same low mortality rate (Run 4). While changing the nutrient uptake formulation has an effect mostly on horizontal variability, changing the zooplankton grazing rate (which is a top-down control) results in a significant change of time variability in the phytoplankton dynamics. In Figure 15 we show the phytoplankton and zooplankton biomass variability for Run 3, Run 4 and the reference simulation (Run 1) within river influenced waters (*SSS* < 16 psu, which was slightly decreased from the SSS limit of 17 psu used in Figure 7, because the differences between the model runs are more apparent toward the more productive areas). Assigning a constant value for K_Z = 0.5 mmol N/m^3 results in the appearance of a zooplankton biomass oscillation that brings phytoplankton biomass to

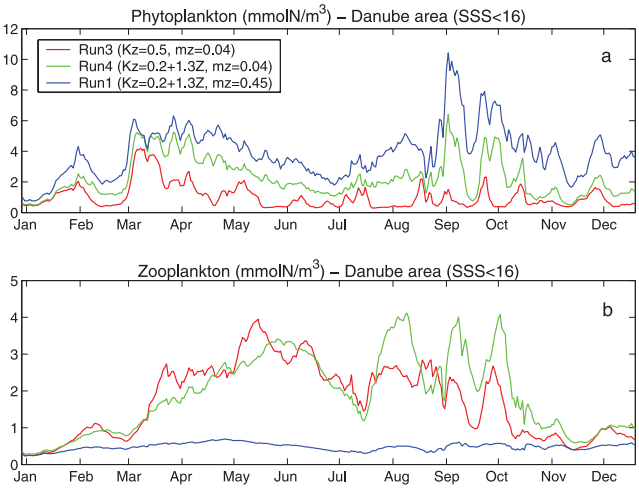

Figure 15. (a) Phytoplankton (mmol N/m^3) and (b) Zooplankton (mmol N/m^3) biomass variability, averaged within the Danube plume area (*SSS* < 16 psu) and over the MiXing Layer Depth (MXLD), as simulated by Run 3 that adopts the parameters (K_Z = 0.5, m_z = 0.04) (red line), Run 4 that adopts the parameters (K_Z = 0.2 + 1.3 *Z*, m_z = 0.04) (green line) and the reference simulation (Run 1, blue line).

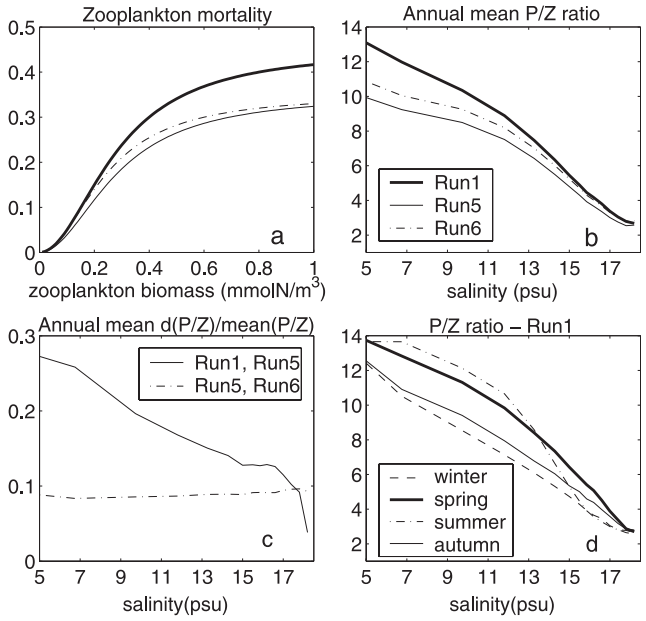

Figure 16. (a) Zooplankton mortality as a function of zooplankton biomass for Run 1 (m_z = 0.45, K_{mz} = 0.08, solid thick line), Run 5 (m_z = 0.35, K_{mz} = 0.06, solid line) and Run 6 (m_z = 0.35, K_{mz} = 0.08, dash-dot line), (b) annual mean P/Z ratio variation with salinity for Run 1, Run 5, Run 6, (c) normalized difference of simulated P/Z ratios (Run 1–Run 6: solid line, Run 5–Run 6: dash-dot line) and (d) seasonal mean P/Z ratio variation with salinity for Run 1.

almost extinction (prevented only by the assigned threshold concentration for grazing). This type of pathological behavior is prevented in Run 4 where K_Z increases with zooplankton concentration. Notice that in Run 3, even though a stronger grazing pressure is assigned (resulting from the lower K_Z = 0.5 mmol N/m^3), the zooplankton biomass attains lower values than Run 4 after August, due to the previously suppressed phytoplankton biomass. The phytoplankton extinction in Run 3 would be easily prevented by choosing a much higher value for K_Z, which, however, would result in an underestimation of grazing rate in the open sea area. One should also notice that the effect of using a lower zooplankton mortality rate by about 10 times results in an about twofold reduction of phytoplankton biomass (compare Run 4 to Run 1 in Figure 15). Even though the impact of the zooplankton grazing formulation is rather small under the adopted high zooplankton mortality rates, the "ratio dependent" grazing formulation seems more robust and provides an additional "bottom-up" stabilizing mechanism even for a decreased zooplankton mortality rate.

[70] In order to demonstrate the impact of grazing pressure on phytoplankton dynamics and the model sensitivity to zooplankton mortality parameters (m_z, K_{mz}), we performed 2 additional simulations: Run5 (m_z = 0.35, K_{mz} = 0.06) and Run6 (m_z = 0.35, K_{mz} = 0.08); the reference simulation Run1 employs (m_z = 0.45, K_{mz} = 0.08). The variation of the mortality function for all 3 cases with zooplankton biomass is shown is Figure 16a. In Figure 16b we present the annual average P/Z ratio for all 3 simulations as a function of salinity, indicating the variation of grazing pressure from the highly eutrophic riverine waters to the open sea. We should note that the region within the salinity range 0–10 psu cannot be considered as representative of the ecosystem functioning as this is the area of immediate river outflow where phytoplankton and zooplankton values are not properly defined. The simulated P/Z ratio varies from about 11–15 in the river end to about 2.5 in the open sea area. Values of P/Z $\sim$ 10–30 within the more eutrophic river influenced waters can be considered as representative of a healthy ecosystem functioning (Violeta Velikova, personal communication); during the 1980s intense eutrophication period P/Z values of >100 were recorded [*Velikova et al.*, 2005]. One may notice that the P/Z ratio of the reference simulation Run 1 falls to the Run 5 simulated P/Z ratio for S > 15 as the two zooplankton mortality functions converge for lower zooplankton biomass values (Figure 16a) due to the higher K_{mz} = 0.08 value adopted for Run 1. In Figure 16c we present the normalized difference in the simulated P/Z ratios. As expected, the difference between Run 1 and Run 6, which is indicative of the model sensitivity to the parameter m_z, is as expected higher in the more eutrophic areas where the mortality function approaches its maximum (Figure 16a) for the higher zooplankton biomass ($\sim$0.6 mmolN/m^3). In contrast, the sensitivity for K_{mz} that is revealed by comparing Run5 and Run6 is higher in the open sea areas, since K_{mz} has a greater impact for lower zooplankton values. In Figure 16d we show the seasonally mean P/Z ratios for the reference simulation. The highest grazing pressure (lower P/Z ratio) is exerted during periods of increased phytoplankton growth limitation. Therefore, the lower P/Z ratio in the river influenced areas is found during winter due to the increased light limitation that results in reduced primary production (as compared to the summer period), while in the open sea areas a lower P/Z ratio is simulated during summer due to severe nutrient limitation. Similarly, higher P/Z ratios are simulated during summer in river-influenced areas and during spring/autumn in the open sea areas.

[71] The most significant deviations of model simulated Chl-a from the SeaWiFS patterns in the open sea area were an overestimation during the spring bloom period and an underestimation during the autumn bloom period (Figures 8 and 9). As already mentioned, we have attributed this model deviation for both cases to model limitations in the parameterization of vertical mixing. For the case of spring we account the excessive vertical mixing, that results in an overestimation of the entrainment of nitrates from the subsurface pool during winter, to the coarse vertical resolution. In order to examine the impact of vertical resolution we performed a similar simulation of the hydrodynamic model but with slightly higher resolution (20 sigma-levels instead of 16). Indeed, as shown in Figure 17a the reference simulation which has lower resolution exhibits a significantly higher MiXing Layer Depth (MXLD, defined in the phytoplankton growth discussion section) from December to February with the difference reaching $\sim$30 m during December, while differences are negligible during the summer stratified period. Therefore we would expect that adopting a

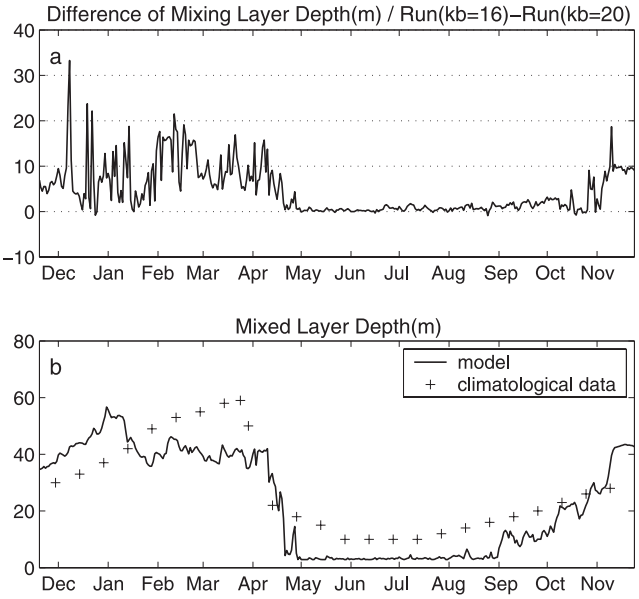

Figure 17. (a) Difference in the simulated MiXing Layer Depth (MXLD) of the control run (16 sigma levels) from the run with higher vertical resolution (20 sigma levels); (b) Mixed Layer Depth (MLD) as simulated by the model control run (continuous line) and from climatological data (Emin Ozsoy, unpublished data; redrawn from *Oguz et al.* [1996]); all values in (m).

higher vertical resolution for the coupled model would significantly eliminate the simulated overestimation during spring. In Figure 17b we have also plotted the model simulated Mixed Layer Depth (MLD, calculated as the depth where a temperature difference of 0.2°C from the surface occurs following *Thompson* [1976]), as compared with climatological data (Emin Oszoy, unpublished data). The model simulated MLD is slightly higher during the December–January period and lower during the February–March period. The steeper decline of the model MLD in the beginning of May can be related to the very weak wind-forcing during the same period (Figure 3b), but the model simulated MLD is also much shallower (<5 m) during the summer-autumn period, which indicates a general underestimation of vertical mixing during the more stratified periods. Episodic mixing due to shear instabilities at the base of the strongly stable thermocline has been recognized as a significant additional mechanism of vertical mixing [*Large et al.*, 1994] that is not taken into account by the Mellor-Yamada turbulence scheme. *Kantha and Clayson* [1994] have shown that introducing a parameterization for this type of mixing at the base of the mixed layer results in a more realistic description of the mixed layer variability. Given that the Black Sea seasonal stratification is enhanced by a very strong halocline, we would expect that the representation of such a shear-induced mixing would significantly improve the simulated mixed layer dynamics during the summer/autumn periods and therefore result in a more pronounced autumn bloom.

[72] The underestimation of Chl-a in the North Romanian shelf area in the beginning of March (Figures 8c and 8d), was the most important deviation of model simulated chlorophyll-a from the observed patterns in the coastal river influenced areas, except some cases that were related to the inaccurate simulation of ISM during light limitation periods (Figures 8a, 8b, 8s, and 8t). In Figure 18 we show the impact of adopting higher or lower attenuation coefficient values (Run 7, k_s = 0.03, Run 8, k_s = 0.11; Run 1 has k_s = 0.07) or a higher N/P stoichiometry (Run 9, $R_{N/P}$ = 20; Run 1 has $R_{N/P}$ = 16) for phytoplankton and zooplankton. In the case of a lower attenuation coefficient (Run 7, Figure 18a), the phytoplankton growth rate (Figure 18c) is significantly increased during winter due to the weaker light limitation, leading to a peak of phytoplankton concentration in the beginning of February that starts declining afterward due to the depletion of phosphates (Figure 18b). The opposite is shown for Run 8 with higher attenuation coefficient (Figure 18a), which exhibits a peak of both growth rate and phytoplankton biomass (Figures 18c and 18d) in early March, all though this peak does not exceed the one by the reference Run 1. Therefore all three cases converge toward the same concentration in early March, although

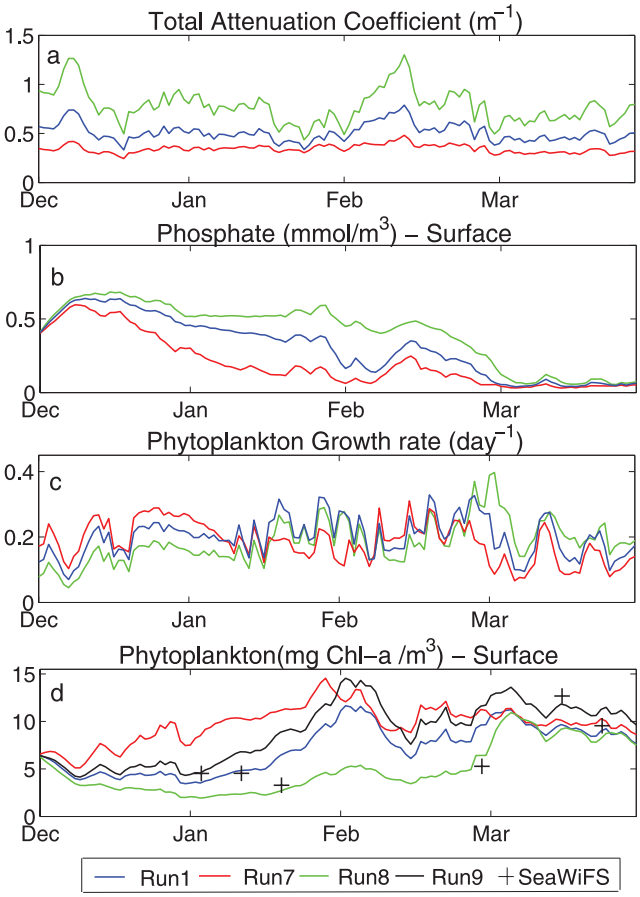

Figure 18. North Romanian shelf area (marked as E in Figure 1) average of (a) total attenuation coefficient (m^{-1}) as simulated by the reference simulation Run1 (blue line, k_s = 0.07), Run 7 (red line, k_s = 0.03) and Run 8 (green line, k_s = 0.11), (b) phosphate (mmol/m^3) (c) phytoplankton growth rate (day^{-1}) for the same runs, (d) phytoplankton concentration (mg Chl-a/m^3) for Run 1 (blue line), Run 7 (red line), Run 8 (green line), Run 9 (black line, $R_{N/P}$ = 20) and from available 8-day SeaWiFS images (Figure 8).

following a different dynamical evolution. The intermediate k_s value of the reference simulation gives the best fit to SeaWiFS Chl-a during January, while the higher k_s value results in a closer agreement with SeaWiFS in late February. A similar analysis also applies with assigning a weaker or stronger temperature dependence (Q10 = 2.2, Q10 = 1.5, not shown) on maximum growth rate, even though with much less pronounced differences from the reference simulation (Q10 = 1.88). The only case that exhibits a significantly stronger biomass in early March is the one with a higher N/P stoichiometric ratio (Run 9, Figure 18d). The growth rate and phosphate levels for this run (not shown) are quite similar to the reference run. However, the lower phosphorus demand that is imposed by the higher N/P phytoplankton stroichiometry may sustain a higher phytoplankton stock. We have also tested the case with a higher N/P ratio of (20) only for zooplankton (by adopting a slightly lower herbivore assimilation efficiency for phosphorus Γ_P = 16/20 * Γ), which however had not a significant impact on phytoplankton biomass, due to the relatively high P/Z ratio in the phosphate limited eutrophic areas. We should note that the assigned N/P ratio stoichiometry value for phytoplankton or zooplankton biomass has an impact mostly in phosphorus-limited areas, as it only enters in phosphorus-related equations.

5. Conclusions

[73] A three-dimensional coupled model of the Western Black Sea plankton dynamics was developed and implemented for the 2003 period using high-resolution/high-frequency forcing, in terms of air-sea interactions and Danube river inputs. A series of 8-day averaged Chl-a SeaWiFS images provided a valuable validation tool that guided us to the improvement of model parameterizations and the calibration of the biological parameters, while groundtruthing was made possible with in situ measurements. The simulation of the seasonal phytoplankton variability over the entire Western Black Sea, extending from the highly eutrophic river influenced area to the open sea area, was a major challenge that made necessary the representation of both the spatial and time variability of several processes. Including phosphorus as a model compartment permitted a more realistic simulation of the P-limited river influenced waters. Adopting a variable function for the zooplankton mortality rate induced from higher predators pressure, resulted in a more realistic variability of the grazing pressure across the productivity gradient. The adoption of a variable function for remineralization rate, as well as the parameterized interaction with the sediment by means of a simple benthic model, permitted the simulation of the observed increased production in coastal areas. The adoption of a variable half-saturation function for nutrient uptake was shown to better describe phytoplankton growth across the significant nutrient gradients. A ''ratio-dependent'' formulation was adopted for zooplankton grazing, which, even though has no significant impact under the adopted high zooplankton mortality rates, seems more robust and provides an additional ''bottom-up'' stabilizing mechanism. The inclusion of ISM as a state variable permitted a more realistic simulation of the light conditions in coastal areas during winter.

[74] The main findings evolve around the strong interaction between physical and biological processes. The advection of low salinity, high nutrient waters that are due to riverine freshwater and nutrient loads (particularly those from the Danube River) largely controls the circulation patterns and productivity on the Northwestern Black Sea shelf. The development of a comprehensive, three-dimensional hydrodynamic model with river plume dynamics and the employment of high-frequency forcing for atmospheric parameters and river loads permitted a satisfactory representation of the variability in the transport pathways of the Danube influenced waters. The coupled model simulations represented several important biophysical processes in both coastal and open seawaters.

[75] Despite the model simplicity, the simulated Chl-a patterns presented a good agreement as compared to the SeaWiFS images. The most noticeable differences were observed in the open sea area, consisting of an overestimation during spring and an underestimation during the autumn periods, which can be attributed to model limitations in the parameterization of vertical mixing. An additional cause could be the over simplistic seasonal variability of zooplankton mortality induced by higher predators. A subsurface chlorophyll maximum was simulated in the open sea area at a depth of $\sim$30–35m, in agreement with existing observations. Agreement between model and observations was best in the coastal areas that were the focus of this study. During winter, phytoplankton in coastal areas was shown to be limited by light availability mostly due to the increased particulate matter concentrations, as a result of resuspension from the sediment and the increased river loads. During summer, the primary production was mostly sustained by riverine nutrients and regeneration processes and thus was strongly linked to the evolution of the Danube plume.

[76] Phosphorus limited areas were shown to extend from the Danube prodelta to the Turkish coast during the winter and spring periods, according to the river pathways and the high N/P ratio of river loads. During summer and autumn periods, the P-limited area was confined in the Danube front area, as the river load N/P ratio was greatly reduced and the benthic fluxes of dissolved nutrients favored N-limitation. The model simulated Chl-a presented a reasonably good agreement with in situ data in the Danube front and the Romanian shelf areas. The limiting nutrients, however, showed deviations from the observed concentrations, indicating the necessity for a more realistic phytoplankton growth model. Another future model upgrade is the inclusion of bacterial dynamics which will enhance our understanding for remineralisation processes.

[77] **Acknowledgments.** The study was funded by the CEC Contract EU Fifth Framework Programme – Energy, environment and sustainable development, Contract No. EVK1-CT-2000-00051: NUtrient management in the DAnube basin and its impact on the Black Sea (DANUBS). We are grateful to Anastasios Papadopoulos of the Hellenic Center for Marine Research, who provided the 2002–2003 POSEIDON atmospheric fields, as well as to Adrianna Cociacu of the National Institute for Marine Research and Development ''Grigore Antipa'', Romania and Violeta Velikova of the Institute of Fisheries and Aquaculture, Varna, Bulgaria, who provided us

with in situ data. Danube daily discharge rates and nutrient loads were kindly provided by Adrian Constantinescu of the Danube Delta National Institute for Research and Development, Tulcea, Romania. The SeaWiFS ocean color data were obtained from NASA's Goddard Space Flight Centre (GSFC-DAAC).

References

Arditi, R., and H. R. Akcakaya (1990), Underestimation of mutual interference of predators, *Oecologia*, *83*, 358–361.

Arditi, R., and L. R. Ginzburg (1989), Coupling in predator-prey dynamics: Ratio-dependence, *J. Theor. Biol.*, *139*, 311–326.

Beers, J. R. (1966), Studies on the chemical composition of the major zooplankton groups in the Sargasso Sea off Bermuda, *Limnol. Oceanogr.*, *11*, 520–528.

Blumberg, A. F., and G. L. Mellor (1983), Diagnostic and prognostic numerical circulation studies of the South Atlantic Bight, *J. Geophys. Res.*, *88*(C8), 4579–4592.

Burban, P. Y., W. Lick, and J. Lick (1989), The flocculation of fine-grained sediments in estuarine waters, *J. Geophys. Res.*, *94*(C6), 8323–8330.

Button, D. K. (1978), On the theory of microbial growth kinetics by limiting nutrient concentrations, *Deep Sea Res.*, *25*, 1163–1177.

Cociacu, A., V. Diakonu, L. Popa, L. Buga, I. Nae, L. Doragan, and V. Malciu (1997), The nutrient stock of the Romanian shelf of the Black Sea during the last three decades, in *Sensitivity to Change: Black Sea, Baltic Sea and North Sea*, *NATO Sci. Ser. 2*, vol. 27, edited by E. Ozsoy and A. Mikaelyan, pp. 49–63, Kluwer Acad., Norwell, Mass.

Cokasar, T., and E. Ozsoy (1998), Comparative analyses and modelling for regional ecosystems of the Black Sea, in *Ecosystem Modelling as a Management Tool for the Black Sea*, *NATO Sci. Ser. 2*, vol. 47, edited by L. Ivanov and T. Oguz, pp. 323–358, Kluwer Acad., Norwell, Mass.

Constantinescu, A., and G. A. M. Menting (2000), Ecological gradients in the Danube Delta lakes, present state and man-induced changes, chapter 3: Hydrology, DDNI and RIZA, Report 2000.015, ISBN 90.369.5309x, Netherlands.

Contois, D. E. (1959), Kinetics of bacterial growth: Relationship between population density and specific growth rate of continuous cultures, *J. Gen. Microbiol.*, *21*, 40–50.

DeAngelis, D. L., R. A. Goldstein, and R. V. O'Neill (1975), A model for trophic interactions, *Ecology*, *56*, 881–892.

Di Toro, D. M., and W. F. Matystik (1980), Mathematical Models of Water Quality in Large Lakes, Part 1: Lake Huron and Saginaw Bay, EPA-600/3-80-056, pp. 28–30.

Droop, M. R. (1968), Vitamin B12 and marine ecology. IV. The kinetics of uptake, growth and inhibition in Monochrysis lutheri, *J. Mar. Biol. Assoc. U. K.*, *48*, 469–733.

Dugdale, R. C. (1967), Nutrient limitation in the sea: Dynamics, identification and significance, *Limnol. Oceanogr.*, *12*, 685–695.

Dyer, K. R. (1989), Sediment processes in estuaries: Future research requirements, *J. Geophys. Res.*, *94*(C10), 14,327–14,339.

Edwards, A. M., and A. Yool (2000), The role of higher predation in plankton population models, *J. Plankton Res.*, *22*, 1085–1112.

Eeckhout, D. V., and C. Lancelot (1997), Modeling the functioning of the northwestern Black Sea ecosystem from 1960 to present, in *Sensitivity to Change: Black Sea, Baltic Sea and North Sea*, *NATO Sci. Ser. Partnership Sub-ser. 2*, vol. 27, edited by E. Ozsoy and A. Mikaelyan, pp. 455–469, Kluwer Acad., Norwell, Mass.

Eppley, R. W. (1972), Temperature and phytoplankton growth in the sea, *Fish. Bull.*, *70*, 1063–1085.

Eppley, R. W., J. N. Rogers, and J. J. McMarthy (1969), Half-saturation constants for uptake of nitrate and ammonium by marine phytoplankton, *Limnol. Oceanogr.*, *14*, 912–920.

Fasham, M., H. Ducklow, and S. McKelvie (1990), A nitrogen-based model of plankton dynamics in the oceanic mixed layer, *J. Mar. Res.*, *48*, 591–639.

Feldman, G. C., and C. R. McClain (2006), Ocean color web, SeaWiFS and MODIS Aqua data, NASA Goddard Space Flight Center, edited by N. Kuring and S. W. Bailey, http://oceancolor.gsfc.nasa.gov/, December.

Finenko, G. A., A. Romanova, G. I. Abolmasova, B. E. Anninsky, L. S. Svetlichny, E. S. Hubareva, L. Bat, and A. E. Kideys (2003), Ingestion, growth and reproduction rates of the alien Beroe ovata and its impacts on the plankton community in the Black Sea, *J. Plankton Res.*, *25*, 539–549.

Flather, R. A. (1976), A tidal model of the Northwest European continental shelf, *Societe Royale de Sciences de Liege, Ser. 6*, *10*, 141–164.

Friedl, G., C. Dinkel, and B. Wehrli (1998), Benthic fluxes of nutrients in the northwestern Black Sea, *Mar. Chem.*, *62*, 77–88.

Friedrich, J., C. Dinkel, G. Friedl, N. Pimenov, J. Wijsman, M.-T. Gomoiu, A. Cociasu, L. Popa, and B. Wehrli (2002), Benthic nutrient cycling and diagenetic pathways in the North Western Black Sea, *Estuarine Coastal Shelf Sci.*, *54*, 369–383.

Fu, G., K. S. Baith, and C. R. McClain (1998), SeaDAS: The SeaWiFS Data Analysis System, Proceedings of The 4th Pacific Ocean Remote Sensing Conference, Qingdao, China, 28–31 July, pp. 73–79.

Garber, J. H. (1984), Laboratory study of nitrogen and phosphorus remineralization during the decomposition of coastal plankton and seston, *Estuarine Coastal Shelf Sci.*, *18*, 685–702.

Geider, R. J., H. L. MacIntyre, and T. M. Kana (1998), A dynamic regulatory model of phytoplanktonic acclimation to light, nutrients and temperature, *Limnol. Oceanogr.*, *43*, 679–694.

Gils, J. van, H. Behrendt, A. Constantinescu, K. Isermann, and M. Zessner (2005), Future development of nutrient emissions and river loads in the Danube Basin, Proceedings of the River Basin Management Conference, Budapest, pp. 219–230.

Ginzburg, L. R., and H. R. Akcakaya (1992), Consequences of ratio-dependent predation for steady state properties of ecosystems, *Ecology*, *73*, 1536–1543.

Goldman, J. C., D. A. Caron, and M. R. Dennett (1987), Regulation of gross growth efficiency and ammonium regeneration in bacteria by substrate C:N ratio, *Limnol. Oceanogr.*, *32*, 1239–1252.

Gregoire, M., and J. Friedrich (2004), Nitrogen budget of the nortwestern Black Sea shelf inferred from modelling studies and in situ benthic measurements, *Mar. Ecol. Prog. Ser.*, *270*, 15–30.

Gregoire, M., J. M. Beckers, J. C. J. Nihoul, and E. Stanev (1998), Reconnaissance of the main Black Sea's ecohydrodynamics by means of a 3D interdisciplinary model, *J. Mar. Syst.*, *16*, 85–105.

Gregoire, M., K. Soetaert, N. Nezlin, and A. Kostianoy (2004), Modelling the nitrogen cycling and plankton productivity in the Black Sea using a three-dimensional interdisciplinary model, *J. Geophys. Res.*, *109*, C05007, doi:10.1029/2001JC001014.

Grill, E. V., and F. A. Richards (1964), Nutrient regeneration from phytoplankton decomposing in seawater, *J. Mar. Res.*, *22*, 51–59.

Guan, W. B., L. A. Wong, and D. F. Xu (2001), Modeling nitrogen and phosphorus cycles and dissolved oxygen in the Pearl River (Zhujiand) Estuary. I. Model development, *Acta Oceanol. Sin.*, *20*, 71–82.

Gucu, A. C. (2002), Can overfishing be responsible for the successful establishment of Mnemiopsis leidyi in the Black Sea?, *Estuarine Coastal Shelf Sci.*, *54*, 439–451.

Harrison, W. G. (1978), Experimental measurements of nitrogen remineralization in coastal waters, *Limnol. Oceanogr.*, *23*, 684–694.

Hasset, R. P., B. Cardinale, L. B. Stabler, and J. J. Elser (1997), Ecological stoichiometry of N and P in pelagic ecosystems: Comparison of lakes and oceans with emphasis on the zooplankton-phytoplankton interaction, *Limnol. Oceanogr.*, *42*, 648–662.

Hellermann, S., and M. Rosenstein (1983), Normal wind stress over the world ocean with error estimates, *J. Phys. Oceanogr.*, *13*, 1093–1104.

Holling, C. S. (1959), Some characteristics of simple types of predation and parasitism, *Can. Entomol.*, *91*, 385–398.

Hopkinson, C. S., Jr., J. J. Vallino, and A. Nolin (2002), Decomposition of dissolved organic matter from the continental margin, *Deep Sea Res., Part II*, *49*, 4461–4478.

Humborg, C. (1997), Primary productivity regime and nutrient removal in the Danube estuary, *Estuar. Coast and Shelf Sci.*, *45*, 579–589.

Jassby, A. D., and T. Platt (1976), Mathematical formulation of the relationship between photosynthesis and light for phytoplankton, *Limnol. Oceanogr.*, *21*, 540–547.

Jost, C. (2000), Predator-prey theory: Hidden twins in ecology and microbiology, *Oikos*, *90*, 202–208.

Kantha, L. H., and C. A. Clayson (1994), An improved mixed layer model for geophysical applications, *J. Geophys. Res.*, *99*(C12), 25,235–25,266.

Karl, D. M., and G. A. Knauer (1991), Microbial production and particle flux in the upper 350 m of the Black Sea, *Deep Sea Res.*, *38*, S921–S942, Suppl. 2.

Kideys, A. E. (2002), Fall and rise of the Black Sea ecosystem, *Science*, *297*, 1482–1484.

Knauer, G. A., J. H. Martin, and K. W. Bruland (1979), Fluxes of particulate carbon, nitrogen and phosphorus in the upper water column of the northeast Pacific, *Deep Sea Res.*, *26A*, 97–108.

Kohlmeier, C., and W. Ebenhoh (1995), The stabilising role of cannibalism in a predator-prey system, *Bull. Math. Biol.*, *57*, 401–411.

Kondo, J. (1975), Air-sea bulk transfer coefficients in diabatic conditions, *Boundary Layer Meteorol.*, *9*, 91–112.

Konovalov, S. K., and J. W. Murray (2001), Variations of the chemistry of the Black Sea on a time scale of decades (1960–1995), *J. Mar. Syst.*, *31*, 243–271.

Konovalov, S., J. W. Murray, and G. W. Luther III (2005), Basic processes of Black Sea biogeochemistry, *Oceanography*, *8*, 25–35.

Korotaev, G., T. Oguz, A. Nokiforov, and C. Koblinsky (2003), Seasonal, interannual and mesoscale variability of the Black Sea upper layer circulation derived from altimeter data, *J. Geophys. Res.*, *108*(C4), 3122, doi:10.1029/2002JC001508.

Kourafalou, V. H., and E. V. Stanev (2001), Modelling the impact of atmospheric and terrestrial inputs on the western Black Sea coastal dynamics, *Ann. Geophys.*, *19*, 245–256.

Kourafalou, V. H., L.-Y. Oey, J. D. Wang, and T. N. Lee (1996), The fate of river discharge on the continental shelf. Part I: Modeling the river plume and the inner-shelf coastal current, *J. Geophys. Res.*, *101*(C2), 3415–3434.

Kourafalou, V. H., K. P. Tsiaras, and J. Staneva (2004), Numerical studies on the dynamics of the Nortwestern Black Sea shelf, *Med. Mar. Sci.*, *5/1*, 133–142.

Krone, R. B. (1962), Flume studies of the transport of sediment in estuarial shoaling processes, Report of Hydraulic Engineering Laboratory and Sanitary Engineering Research, 110 University of California, Berkeley.

Lancelot, C. L., J. V. Staneva, D. Van Eeckhout, J.-M. Beckers, and E. V. Stanev (2002), Modelling the Danube-influenced North-western continental shelf of the Black Sea. Ecosystem response to changes in nutrient delivery by the Danube River after its damming in 1972, *Estuarine Coastal Shelf Sci.*, *54*, 473–499.

Large, W. G., J. C. McWilliams, and S. Doney (1994), Oceanic vertical mixing: A review and a model with a nonlocal boundary layer parameterization, *Rev. Geophys.*, *32*, 363–403.

Lebedeva, L. P., and E. A. Shushkina (1994), Modeling the effect of Mnemiopsis on the Black Sea plankton community, *Oceanology, Engl. Transl.*, *34*, 72–80.

Lorenzen, C. J. (1972), Extinction of light in the ocean by phytoplankton, *J. Cons. Cons. Int. Explor. Mer*, *34*, 262–267.

MacIsaac, J. J., and R. C. Dugdale (1969), The kinetics of nitrate and ammonia uptake be natural populations of marine phytoplankton, *Deep Sea Res.*, *16*, 415–422.

McClain, C., G. Feldman, and S. Hooker (2004), An overview of the SeaWiFS project and strategies for producing a climate research quality global ocean bio-optical time series, *Deep Sea Res., Part II*, *51*(1–3), 5–42.

McClain, C., S. Hooker, G. Fledman, and P. Bontempi (2006), Satellite data for ocean biology, biogeochemistry and climate research, *Eos Trans. AGU*, *87*(34), 337–343.

Mellor, G. L., and T. Yamada (1982), Development of a turbulence closure model for geophysical fluid problems, *Rev. Geophys. Space Phys.*, *20*, 851–875.

Monod, J. (1942), *Recherches sur la croissance des cultures bacteriennes*, 2nd ed., 211 pp., Hermann, Paris,

Morrisson, K. A., N. Therien, and B. Macros (1987), Comparison of six models for nutrient limitations on phytoplankton growth, *Can. J. Fish. Aquat. Sci.*, *44*, 1278–1288.

Murray, J. W., H. W. Jannasch, S. Honjo, R. F. Anderson, W. S. Reeburgh, Z. Top, G. E. Friedrich, L. A. Codispoti, and E. Izdar (1989), Unexpected changes in the oxic/anoxic interface in the Black Sea, *Nature*, *338*, 411–413.

Murray, J. W., C. Fuchsman, J. Kirpatrick, B. Paul, and S. Konovalov (2005), Species and δ^{15} signature of nitrogen transformations in the suboxic zone of the Black Sea, *Oceanography*, *18*, 36–47.

Nittis, K., L. Perivoliotis, G. Korres, C. Tziavos, and I. Thanos (2006), Operational monitoring and forecasting for marine environmental applications in the Aegean Sea, *Environ. Modell. Software*, *21*, 243–257.

Oguz, T., and P. Malanotte-Rizzoli (1996), Seasonal variability of wind and thermohaline driven circulation in the Black Sea: Modelling studies, *J. Geophys. Res.*, *101*(C7), 16,551–16,569.

Oguz, T., and B. Salihoglou (2000), Simulation of eddy-driven phytoplankton production in the Black Sea, *Geophys. Res. Lett.*, *27*(14), 2125–2128.

Oguz, T., P. E. LaViolette, and U. Unluata (1992), The upper layer circulation of the Black Sea: Its variability as inferred from hydrographic and satellite observations, *J. Geophys. Res.*, *97*(C8), 12,569–12,584.

Oguz, T., P. Malanotte-Rizzoli, and D. G. Aubrey (1995), Wind and thermohaline circulation of the Black Sea driven by yearly mean climatological forcing, *J. Geophys. Res.*, *100*(C4), 6845–6863.

Oguz, T., H. Ducklow, P. Malanote-Rizzoli, S. Turgul, N. Nezlin, and U. Unluata (1996), Simulation of annual plankton cycle in the Black Sea by a one-dimensional physical biological model, *J. Geophys. Res.*, *101*(C4), 16,551–16,569.

Oguz, T., H. Ducklow, E. A. Shushkina, P. Malanote-Rizzoli, S. Turgul, and L. P. Lebedeva (1998), Simulation of upper layer biogeochemical structure in the Black Sea, in *Ecosystem Modelling as a Management tool for the Black Sea*, *NATO Sci. Ser. 2*, vol. 47, edited by L. Ivanov and T. Oguz, pp. 323–358, Kluwer Acad., Norwell, Mass.

Oguz, T., H. Ducklow, P. Malanotte-Rizzoli, J. W. Murray, V. I. Vedernikov, and U. Unluata (1999), A physical-biochemical model of plankton productivity and nitrogen cycling in the Black Sea, *Deep Sea Res., Part I*, *46*, 597–636.

Oguz, T., H. W. Ducklow, and P. Malanotte-Rizzoli (2000), Modelling distinct vertical biogeochemical structure of the Black Sea: Dynamical coupling of the oxic, suboxic and anoxic layers, *Global Biogeochem. Cycles*, *14*(4), 1331–1352.

Oguz, T., H. W. Ducklow, J. E. Purcell, and P. Malanotte-Rizzoli (2001a), Modelling the response of top-down control exerted by gelatinous carnivores on the Black Sea pelagic food web, *J. Geophys. Res.*, *106*(C3), 4543–4564.

Oguz, T., J. W. Murray, and A. E. Callahan (2001b), Modeling redox cycling across the suboxic-anoxic interface zone in the Black Sea, *Deep Sea Res., Part I.*, *48*, 761–787.

Oguz, T., A. G. Deshpande, and P. Malanotte-Rizzoli (2002), On the role of mesoscale processes controlling biological variability in the Black Sea: Inferences from SeaWiFS-derived surface chlorophyll field, *Cont. Shelf Res.*, *22*, 1477–1492.

O'Reilly, J. E., et al. (2000), Ocean color chlorophyll-a algorithms for SeaWiFS, OC2 and OC4: Version 4, in *SeaWiFS Postlaunch Calibration and Validation Analyses, Part 3*, *SeaWiFS Postlaunch Technical Report Series*, vol. 11, edited by S. B. Hooker and E. R. Firestone, pp. 9–23, NASA/TM-2000-206892.

Papadopoulos, A., G. Kallos, P. Katsafados, and S. Nickovic (2002), The Poseidon weather forecasting system: An overview, *Global Atmos. Ocean Syst.* (retitled *J. Atmos. Ocean Sci.)*, *8*(2–3), 219–237.

Partheniades, E. (1965), Erosion and deposition of cohesive soils, *J. Hydrol. Div.*, ASCE 91, No. HY1, 105–139.

Ragueneau, O., et al. (2002), Biogeochemical transformations of inorganic nutrients in the mixing zone between the Danube River and the Northwestern Black Sea, *Estuarine Coastal Shelf Sci.*, *54*, 321–336.

Redfield, A. C., B. H. Ketchum, and F. A. Richards (1963), The influence of organisms on the composition of seawater, in *The Sea*, vol. 2, edited by M. N. Hill, pp. 26–77, Interscience, NewYork, N.Y.

Roques, H., H. Yue, S. Saipanich, and B. Capdeville (1982), Faut-il abandonner le formalisme de monod pour la modelisation des processus de de'pollution par voie biologique?, *Water Res.*, *16*, 839–847.

Rosati, A., and K. Miyakoda (1988), A general circulation model for upper ocean circulation, *J. Phys. Oceanogr.*, *18*, 1601–1626.

Ryabchenko, V. A., M. J. R. Fasham, B. A. Kagan, and E. E. Popova (1997), What causes short-term oscillations in ecosystem models of the ocean mixed layer?, *J. Mar. Syst.*, *13*, 33–50.

Saydam, C., S. Tugrul, O. Basturk, and T. Oguz (1993), Identification of the oxic/anoxic interface by isopycnal surfaces in the Black Sea, *Deep Sea Res.*, *40*, 1405–1412.

Schreiber, H., H. Behrendt, L. T. Constantinescu, I. Critevic, D. Drumea, D. Jabucar, S. Juran, B. Pataki, S. Snishko, and M. Zessner (2005), Point and diffuse nutrient emissions and loads in the transboundary Danube River basin: A modelling approach, *Arch. Hydrobiol. Suppl.*, *158/1–2*, *Large Rivers*, *16*(1–2), 197–220.

Shi, Z., and H. J. Zhou (2004), Controls on effective settling of mud flocs in the Changjiang Estuary, China, *Hydrol. Processes*, *18*, 2877–2892.

Stanev, E. V., J. V. Staneva, and V. M. Roussenov (1997), On the Black Sea water mass formation. Model sensitivity study to atmospheric forcing and parameterizations of physical processes, *J. Mar. Syst.*, *13*, 245–272.

Stanev, E. V., J. M. Beckers, C. Lancelot, J. V. Staneva, P. Y. Le Traon, E. L. Peneva, and M. Gregoire (2002), Coastal-open ocean exchange in the Black Sea: Observations and modelling, *Estuarine Coastal Shelf Sci.*, *54*, 601–620.

Staneva, J. V., and E. V. Stanev (1997), Cold water mass formation in the Black Sea and its sensitivity to horizontal resolution in numerical models, in *Sensitivity of North Sea, Baltic Sea and Black Sea to Anthropogenic and Climatic Changes, NATO Sci. Ser. 2*, vol. 47, edited by E. Ozsoy and A. Mikaelyan, pp. 375–393, Kluwer Academic, Norwell, Massachusetts.

Staneva, J. V., and E. V. Stanev (1998), Oceanic response to atmospheric forcing derived from different climatic data sets. Intercomparison study for the Black Sea, *Oceanol. Acta*, *21*, 383–417.

Staneva, J. V., E. V. Stanev, and T. Oguz (1998), The impact of atmospheric forcing and water column stratification on the yearly plankton cycle, in *Ecosystem modelling as a management tool for the Black Sea, NATO Sci. Ser. 2*, vol. 47, edited by T. Oguz and L. Ivanov, pp. 301–323, Kluwer Academic, Norwell, Massachusetts.

Steele, J. H., and E. W. Henderson (1981), A simple plankton model, *Am. Nat.*, *117*, 676–691.

Steele, J. H., and E. W. Henderson (1992), The role of predation in plankton models, *J. Plankton Res.*, *14*, 157–172.

Sverdrup, H. U. (1953), On the conditions for vernal blooming of the phytoplankton, *ICES J. Mar. Sci.*, *18*, 287–295.

Tanguy, D., and M. Loreau (2001), Ecological stoichiometry, primary producer-decomposer interactions and ecosystem persistence, *Ecology*, *82*, 3069–3082.

Tarapchak, S. J., and L. R. Herche (1986), Phosphate uptake by microorganisms in lake water: Deviations from simple Michaelis-Menten kinetics, *Can. J. Fish. Aquat. Sci.*, *43*, 319–328.

Thompson, R. O. R. Y. (1976), Climatological models of the surface mixed layer of the ocean, *J. Phys. Oceanogr.*, *6*, 496–503.

Tilman, D. (1981), Tests of resource competition theory using four species of Lake Michigan algae, *Ecology*, *62*(3), 802–815.

Tolmazin, D. (1985), Changing coastal oceanography of the Black Sea. I: Northwestern Shelf, *Prog. Oceanogr.*, *15*, 217–276.

Tugrul, S., O. Basturk, C. Saydam, and A. Yilmaz (1992), Changes in the hydrochemistry of the Black Sea inferred from water density profiles, *Nature*, *359*, 137–139.

Vedernikov, V. I., and A. B. Demidov (1997), Vertical distribution of primary production and chlorophyll during different seasons in deep regions of the Black Sea, *Oceanology*, *37*, 376–384.

Velikova, V., A. Cociasu, L. Popa, L. Boicenco, and D. Petrova (2005), Phytoplankton community and hydrochemical characteristics of the Western Black Sea, *J. Water Sci. Technol.*, *51*, 27–37.

Vidal, C. V. (1995), Bio-optical characteristics of the Mediterranean and the Black Sea. M.S. thesis, 134 pp., Inst. of Mar. Sci., Middle East Tech. Univ., Endemli, Icel, Turkey.

Vladimirov, V. L., V. I. Mankovsky, M. V. Solokev, and A. V. Mishonov (1996), Seasonal and long term variability of the Black Sea optical parameters, in *Sensitivity of North Sea, Baltic Sea and Black Sea to Anthropogenic and Climatic Changes*, *NATO ASI Ser. 2*, edited by E. Ozsoy and A. Mikaelyan, Kluwer Acad., Norwell, Mass.

Williams, P. J. (1973), The validity of the application of simple kinetic analysis to heterogeneous microbial populations, *Limnol. Oceanogr.*, *18*, 159–165.

Wroblewski, J. (1977), A model of phytoplankton plume formation during variable Oregon upwelling, *J. Mar. Res.*, *35*, 357–394.

Zaitsev, P. Yu., and B. G. Alexandrov (1997), Recent man-made changes in the Black Sea ecosystem, in *Sensitivity of North Sea, Baltic Sea and Black Sea to Anthropogenic and Climatic Changes*, *NATO ASI Ser. 2*, edited by E. Ozsoy and A. Mikaelyan, Kluwer Acad., Norwell, Mass.

A. Davidov, Biological Oceanography/Marine Biogeochemistry, Leibniz-Institute of Marine Sciences – IFM-Geomar, Dusternbrooker Weg 20, 24105, Kiel, Germany. (adavidov@ifm-geomar.de)

V. H. Kourafalou, Division of Meteorology and Physical Oceanography, Rosenstiel School of Marine and Atmospheric Science, University of Miami, 4600 Rickenbacker Cswy., Miami, FL 33149, USA. (vkourafalou@rsmas.miami.edu)

J. Staneva, Institute for Coastal Research, GKSS Research Center, Max Planck Strasse 1, D-21502, Geesthacht, Germany. (joanna.staneva@gkss.de)

K. P. Tsiaras, Institute of Oceanography, Hellenic Center for Marine Research, Athens-Sounio Ave., 46.7 km, P.O. 712, 19013, Anavyssos, Greece. (ktsiaras@ath.hcmr.gr)